Atmospheric
Chemistry
and Physics

On the atmospheric budget of 1,2-dichloroethane and its impact on stratospheric chlorine and ozone (2002–2020)

Ryan Hossaini[1], **David Sherry**[2], **Zihao Wang**[3,4], **Martyn P. Chipperfield**[3,5], **Wuhu Feng**[3,6], **David E. Oram**[7,8], **Karina E. Adcock**[8], **Stephen A. Montzka**[9], **Isobel J. Simpson**[10], **Andrea Mazzeo**[1], **Amber A. Leeson**[1], **Elliot Atlas**[11], and **Charles C.-K. Chou**[12]

[1]Lancaster Environment Centre, Lancaster University, Lancaster, UK
[2]Nolan Sherry and Associates (NSA), London, UK
[3]School of Earth and Environment, University of Leeds, Leeds, UK
[4]Department of Ocean Sciences and Engineering,
Southern University of Science and Technology, Shenzhen, China
[5]National Centre for Earth Observation, University of Leeds, Leeds, UK
[6]National Centre for Atmospheric Science, University of Leeds, Leeds, UK
[7]National Centre for Atmospheric Science, University of East Anglia, Norwich, UK
[8]Centre for Ocean and Atmospheric Science, School of Environmental Sciences,
University of East Anglia, Norwich, UK
[9]NOAA Global Monitoring Laboratory (GML), Boulder, CO, USA
[10]Department of Chemistry, University of California, Irvine, Irvine, CA, USA
[11]Department of Atmospheric Sciences, RSMAES, University of Miami, Miami, FL, USA
[12]Research Center for Environmental Changes, Academia Sinica, Taipei, Taiwan

Correspondence: Ryan Hossaini (r.hossaini@lancaster.ac.uk)

Abstract. The chemical compound 1,2-dichloroethane (DCE), or ethylene dichloride, is an industrial very short-lived substance (VSLS) whose major use is as a feedstock in the production chain of polyvinyl chloride (PVC). Like other chlorinated VSLSs, transport of DCE (and/or its atmospheric oxidation products) to the stratosphere could contribute to ozone depletion there. However, despite annual production volumes greatly exceeding those of more prominent VSLSs (e.g. dichloromethane), global DCE observations are sparse; thus, the magnitude and distribution of DCE emissions and trends in its atmospheric abundance are poorly known. In this study, we performed an exploratory analysis of the global DCE budget between 2002 and 2020. Combining bottom-up data on annual production and assumptions around fugitive losses during production and feedstock use, we assessed the DCE source strength required to reproduce atmospheric DCE observations. We show that the TOMCAT/SLIMCAT 3-D chemical transport model (CTM) reproduces DCE measurements from various aircraft missions well, including HIPPO (2009–2011), ATom (2016–2018), and KORUS-AQ (2016), along with surface measurements from Southeast Asia, when assuming a regionally varying production emission factor in the range of 0.5 %–1.5 %. Our findings imply substantial fugitive losses of DCE and/or substantial emissive applications (e.g. solvent use) that are poorly reported. We estimate that DCE's global source increased by $\sim 45\%$ between 2002 ($349 \pm 61\,\mathrm{Gg\,yr^{-1}}$) and 2020 ($505 \pm 90\,\mathrm{Gg\,yr^{-1}}$), with its contribution to stratospheric chlorine increasing from 8.2 (± 1.5) to ~ 12.9 (± 2.4) pptCl (where ppt denotes parts per trillion) over this period. DCE's relatively short overall tropospheric lifetime ($\sim 83\,\mathrm{d}$) limits, although does not preclude, its transport to the stratosphere, and we show that its impact on ozone is small at present. Annually averaged, DCE is estimated to have decreased ozone in the lower stratosphere by up to several parts per billion ($< 1\%$) in 2020, although a larger effect in the springtime Southern Hemisphere polar lower stratosphere is apparent (decreases of up to

$\sim 1.3\%$). Given strong potential for growth in DCE production tied to demand for PVC, ongoing measurements would be of benefit to monitor potential future increases in its atmospheric abundance and its contribution to ozone depletion.

1 Introduction

Very short-lived substances (VSLSs) are a class of halogenated chemicals with local surface lifetimes of typically less than ~ 6 months, leading to spatial and temporal heterogeneity in their tropospheric abundance (e.g. WMO, 2018, 2022). Despite short lifetimes relative to long-lived ozone-depleting substances (ODSs) controlled by the Montreal Protocol, such as chlorofluorocarbons (CFCs) and hydrochlorofluorocarbons (HCFCs), a range of both natural and anthropogenic VSLSs have been detected in the lower stratosphere (e.g. Laube et al., 2008; Hossaini et al., 2019; Keber et al., 2020). This has motivated research into the possible impacts of VSLSs on stratospheric ozone and ozone trends (e.g. Salawitch et al., 2005; Feng et al., 2007; Falk et al., 2017; Bednarz et al., 2022, 2023; Villamayor et al., 2023). The most prominent VSLSs with significant industrial sources are chlorinated compounds (Cl-VSLSs), including dichloromethane (CH$_2$Cl$_2$) and chloroform (CHCl$_3$). These gases have a non-zero ozone depletion potential (ODP; Claxton et al., 2019), and global emissions of both have increased considerably in recent years, particularly from Asia (e.g. Hossaini et al., 2017; Fang et al., 2019; Say et al., 2019; Claxton et al., 2020; An et al., 2021, 2023).

The molecule 1,2-dichloroethane (CH$_2$ClCH$_2$Cl, DCE), also known commonly as ethylene dichloride (EDC), is a further chlorinated VSLS, produced industrially in large volumes worldwide. In the USA, for instance, ~ 9000–$14\,000$ Gg of DCE is estimated to have been produced annually in the period from 2011 to 2015 (ATSDR, 2024), and the global total production capacity in 2020 was estimated at $\sim 60\,000$ Gg (TEAP, 2022). DCE's main use is as a chemical intermediate in the manufacture of vinyl chloride monomer (VCM), a raw material in the production of the widely used plastic, polyvinyl chloride (PVC). Over 95 % of DCE consumption is estimated to be in VCM production (UNEP, 2002; ECHA, 2012; CEH, 2023) which, in principle, is a largely non-emissive application (i.e. because DCE is consumed in reaction). Like other halocarbons, however, fugitive release of DCE to the atmosphere may occur during its production, storage, and transportation (TEAP, 2022). Other known but relatively minor uses of DCE include the following: (1) in the production of other chemicals, such as ethyleneamines (e.g. Ayres and Ayres, 1997); (2) historically, as a lead scavenger in fuels (e.g. Falta et al., 2005); and (3) in various applications on account of being an effective solvent, such as metal degreasing (EPA, 2020), and in organic and medicinal chemistry (e.g. Jordan et al., 2020). Due to concern over its toxicity, regulatory controls restricting commercial DCE uses are in place in some regions, including the European Union (Sherwood, 2018) where DCE was placed in Annex XIV of the EU's REACH (Registration, Evaluation, Authorisation and Restriction of Chemicals) regulation in 2016.

In contrast to other major chlorinated VSLSs (e.g. CH$_2$Cl$_2$, CHCl$_3$, and C$_2$Cl$_4$), the National Oceanic and Atmospheric Administration (NOAA) and Advanced Global Atmospheric Gases Experiment (AGAGE) global monitoring networks do not yet routinely report surface DCE measurements, and there are no other archived long-term observational records. As a consequence, the global DCE budget and trends in its atmospheric abundance are poorly known. The current paucity of global DCE surface measurements also prevents the assessment of its global source using top-down inverse methods, as performed for other industrial VSLSs (Claxton et al., 2020). Measurements of DCE from a limited number of aircraft campaigns in various world regions indicate typical Northern Hemisphere (NH) boundary layer mole fractions in the range of ~ 10–20 ppt (Engel and Rigby et al., 2018; Roozitalab et al., 2024). However, far larger levels have also been detected in East and Southeast Asia, including mole fractions > 1 ppb in China at both urban and background sites (Lyu et al., 2020, and references therein). Based on air samples obtained from surface sites in Taiwan and Malaysia in 2013 and 2014, Oram et al. (2017) reported median DCE mole fractions of 85.4 (16.7–309) and 21.7 (16.4–120) ppt, respectively, with a strong correlation of DCE with CH$_2$Cl$_2$ observed at both sites. Combining this relationship with a bottom-up estimate of regional CH$_2$Cl$_2$ emissions, the same study inferred Chinese DCE emissions to be of the order of 203 (± 9) Gg yr^{-1} for the period from 2013 to 2014.

Based on a combination of high-altitude aircraft observations and modelling, Cl-VSLSs were estimated to provide ~ 130 (100–160) ppt Cl to the stratosphere in 2019 (Laube and Tegtmeier et al., 2022). Although this represents just $\sim 4\%$ of total stratospheric chlorine (which is principally from long-lived ODSs that are now controlled by the Montreal Protocol), increasing VSLS amounts have slowed the rate at which chlorine is decreasing in the stratosphere (Hossaini et al., 2019; Bednarz et al., 2022). Additionally, far larger local injections of Cl-VSLSs (including DCE) into the Northern Hemisphere (NH) extratropical lower stratosphere (LS) have been reported (Adcock et al., 2021; Lauther et al., 2022), reflecting transport via the Asian summer monsoon anticyclone and the co-location of relatively strong

Asian emissions with efficient vertical ascent (e.g. Randel et al., 2010). While CH$_2$Cl$_2$ remains the largest contributor to stratospheric chlorine from VSLSs (Laube and Tegtmeier et al., 2022), the large volumes of DCE produced worldwide, its substantial global trade, and the potential for future growth tied to PVC demand (e.g. in the building and construction industries) means it is of interest to establish DCE's present-day atmospheric budget and fate.

In this study, we have analysed global DCE production data between 2002 and 2020 and used them to create a set of gridded global emissions for different assumed emission factors describing fugitive DCE losses. Using the TOM-CAT/SLIMCAT 3-D chemical transport model (CTM), we evaluated the realism of these emissions by assessing the model's ability to reproduce various aircraft measurements of DCE, thereby providing new constraints on its global source. The CTM was used to quantify the likely contribution of DCE and its products to stratospheric chlorine and thus the potential impact of DCE emissions on stratospheric ozone. The paper is structured as follows. Section 2 describes our approach to creating the DCE emission inventories, as well as the CTM, the simulations performed, and observational datasets used. Our results are presented in Sect. 3, including on the inferred magnitude of global DCE emissions (Sect. 3.1), DCE's budget and contribution to stratospheric chlorine (Sect. 3.2), and DCE's impact on stratospheric ozone (Sect. 3.3). A summary of key findings and concluding remarks is given in Sect. 4.

2 Data, methods, and model

2.1 Bottom-up data on DCE production

DCE is manufactured industrially via the direct chlorination of ethene or via its oxychlorination with hydrogen chloride. Estimated annual DCE production data were compiled biennially by Nolan Sherry Associates (NSA) over the period from 2002 to 2020 (Table 1). Data from NSA were reported in the most recent Technology and Economic Assessment Panel (TEAP) report to the parties of the Montreal Protocol (TEAP, 2022) and have been utilized in a range of recent scientific papers (e.g. Chipperfield et al., 2018; Claxton et al., 2020). Analysis by NSA makes use of their extensive database of halocarbon production and production capacities, industry data, and public reports, and is refined through industry dialogue. NSA's analysis of DCE production includes assessment of downstream products (VCM and PVC), accounting for several specific industry and market factors and trade movements. This includes the fact that VCM production may not always occur via the "ethylene route", which uses DCE at a rolling ratio of 1.6 units of DCE to VCM, but the "acetylene route", which involves the direct production of VCM from acetylene's reaction with hydrogen chloride (i.e. no DCE involved). The latter approach is prevalent in, for example, China, meaning that Chinese DCE production is rela-

tively modest compared with other major global economies. Note that at the country level, some of the data available to NSA are proprietary in nature and confidential. On this basis and to aid the discussion and presentation, data have been aggregated into 13 broader geographical regions for which we discuss production and emissions. These regions cover all of the world's major industrialized zones, and their boundaries (Fig. 1) are based on the region definitions used in Phase 2 of the Hemispheric Transport of Air Pollution (HTAP) project (e.g. Huang et al., 2017).

Evident from the data in Table 1 is that DCE is produced in large quantities ($\sim$ 52 000 Gg in 2020) and that global production increased by $\sim$ 29 % between 2002 and 2020. US/Canada; Europe; and S, E, and SE Asia (regions 1–5) were estimated to account for $\sim$ 86 % of world production in 2020. Noting that the end product of DCE's principal industrial use (i.e. PVC) is closely followed and reported on by both business performance analysts and environmentalists, the production data from NSA are estimated to be accurate to within around $\pm$ 5 %. Although estimates of DCE production in peer-reviewed literature are scarce, some independent figures exist with which to compare. For instance, data cited by the US Environmental Protection Agency (EPA) placed the annual volume of DCE produced in the USA at 12 750 Gg in 2011 (EPA, 2020). Interpolating between years on either side (recalling that production data from NSA were provided biennially), the corresponding US production from NSA is 13 145 Gg (2011), i.e. in close agreement with the US EPA figure (within $\sim$ 3 %). An assessment around health aspects of DCE exposure placed European production at more than 10 000 Gg yr^{-1} (Cherrie et al., 2011), consistent with the NSA data in Table 1. Few estimates of DCE production in Asia exist in the peer-reviewed literature. However, an estimate of Chinese DCE production in the year 2010 of 2708 Gg (Chinabaogao, 2012) is very similar to that for China from NSA in the same year (2700 Gg).

The demand for DCE in both producing and non-producing countries was evaluated from trade data. Net imports (gross imports minus gross exports) were calculated for a total of $\sim$ 150 countries over our study period (2002–2020) using publicly available trade statistics accessed via the online UN Comtrade Database (https://comtradeplus.un.org/, last access: 22 November 2024). Assuming that global imports should equal global exports in a given year, net imports should sum to zero across the globe. However, due to imperfections in reported trade data (known to afflict many commodities besides DCE), this was not found to be the case. Although the imbalance was small (average of $\sim$ 7 % over our study period, expressed as the difference between gross imports and exports) compared with the large production volumes of DCE, we elected to reconcile the trade data using the method of Zou et al. (2023). Briefly, where a record of DCE trade is recorded by the importer but not the exporter (or vice versa), the missing trade is filled in. Where records match but the trade quantities differ, the larger of the two was adopted

Table 1. Estimated annual production of DCE (Gg) from NSA in the 13 world regions in Fig. 1.

R no.	Region name	2002	2004	2006	2008	2010	2012	2014	2016	2018	2020
1	US/Canada	14 429	14 929	13 894	12 649	12 789	13 499	14 199	16 199	18 199	16 749
2	Europe	11 176	11 757	12 055	11 300	11 680	11 771	11 739	11 799	11 749	11 499
3	S Asia	284	257	239	274	449	479	399	423	457	444
4	E Asia	8951	9545	10 563	10 642	10 771	10 534	10 723	11 738	13 889	14 147
5	SE Asia	1114	1249	1239	1409	1549	1759	1799	2014	2153	2199
6	Australia/NZ	0	0	0	0	0	0	0	0	0	0
7	Africa, north	117	144	144	139	137	224	314	314	339	555
8	Africa, sub-Saharan	207	175	207	151	263	223	263	271	263	239
9	Middle East	1636	1830	2076	1817	2552	2807	2924	3339	3436	3327
10	Central America	394	279	524	579	639	629	609	89	89	89
11	South America	1129	1234	1379	1639	1559	1429	1579	1609	1389	999
12	E Europe/N Asia	1011	976	1294	1274	1214	1034	1179	1359	1819	1889
13	Central Asia.	0	0	0	0	0	0	0	0	0	0
	Global total	40 457	42 384	43 623	41 882	43 611	44 398	45 737	49 164	53 792	52 146
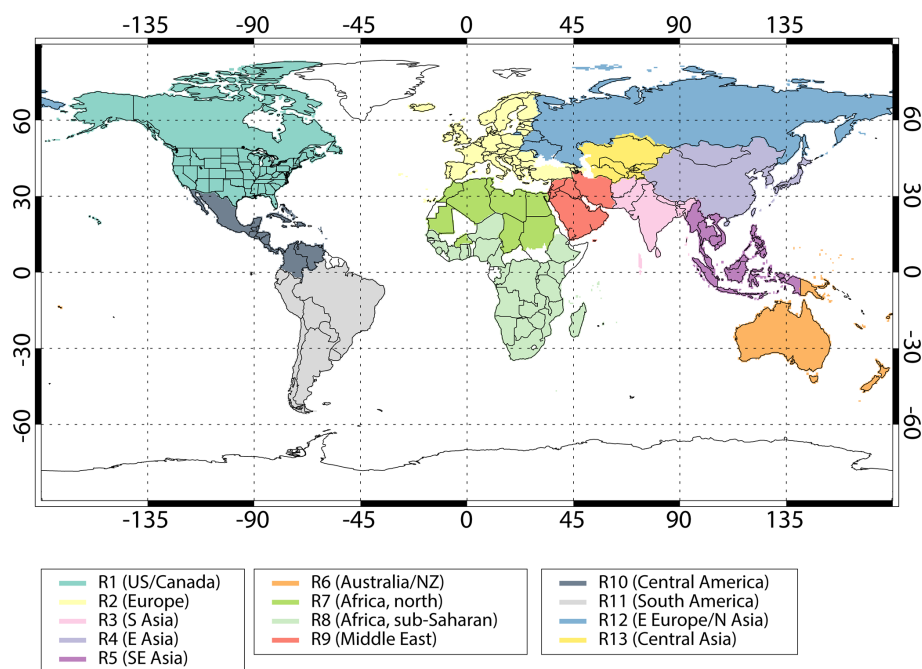
Figure 1. Definitions of the 13 geographical regions considered for DCE production and emissions.

(Zou et al., 2023). This approach balances global DCE trade and prevents errors in trade statistics from confounding our subsequent analysis.

2.2 DCE emissions

In principle, emissions of DCE may arise during its (1) production, (2) use as a feedstock, (3) transportation, and (4) any emissive uses (e.g. as a solvent). Items 1–3 represent fugitive emissions that may arise from, for example, the operation and maintenance of chemical plants, along with bulk storage and other industrial processes where unintended leak-age can occur. In a fully explicit bottom-up inventory, production emissions may be calculated as the product of annual DCE production and a suitable emission factor. Similarly, feedstock use emissions, which are additional and additive, may be calculated from the quantity of DCE used as feedstock and a further emission factor (e.g. TEAP, 2022). However, although DCE is principally used as a feedstock in the manufacture of VCM, with some assessments placing this use at > 98 % (CEH, 2023), the precise quantity and how this may have varied over time and across regions is unknown. Note, even if 98 % of DCE use is in producing VCM, this does not imply that the remaining 2 % is used in

emissive applications. This is because DCE also finds use as an intermediate in the production of other chemicals, including ethyleneamines and other chlorinated solvents (Sect. 1; TEAP, 2022). Analysis by NSA suggests that these two sectors contribute of the order of 600–800 Gg yr^{-1} of DCE feedstock use. In our idealized framework for calculating DCE emissions, we assume that 100 % of DCE use (consumption) is as feedstock.

The annual total DCE emission per country in year t was calculated using Eq. (1).

$$\text{Emission}(t) = P(t)\alpha_1 + C(t)\alpha_2 + I(t)\alpha_3 \qquad (1)$$

The first term on the right denotes production emissions calculated from the temporally varying production (P) data provided by NSA. There are 36 producing countries in the NSA database to which this term applies. The second term on the right denotes feedstock use emissions calculated based on consumption (C) data. Consumption (production + net imports) was calculated for ~150 countries in total. The DCE-producing countries dominate global consumption, with non-producers accounting for less than 0.6 % of the global total. Production and consumption data in Tables 1 and 2 are aggregated regional totals obtained from country-level analysis. The third term on the right of Eq. (1) represents fugitive emissions during the supply chain. We have elected to apply these in the country of import, and they are calculated from gross import (I) data.

In Eq. (1), emission factors for production, feedstock use, and supply chain emissions are denoted by α_1, α_2, and α_3, respectively. Tight emission controls throughout the whole DCE production cycle and its supply chain, especially in more developed countries, are expected to occur to minimize loss of useful material, to control costs in an extremely competitive industry, and also for possible legal compliance. For DCE, all α values in developed countries are thus expected to be small and likely to lie towards the lower end of the plausible ranges reported in the literature for other gases (TEAP, 2022). For context, fugitive emissions from the production of other halocarbons have typically been estimated at ~0.5 % on production (IPCC/TEAP, 2005). However, due to differences in plant operations and regulatory requirements in different world regions, regional differences in emission factors are likely. For DCE, we examined a range of emission factors around the above value, varying α_1 between 0.1 % and 0.6 % for developed countries. For developing countries, approximated as those operating under Article 5 (A5) of the Montreal Protocol, we assume a multiplier of 3. The different scenarios are labelled according to their developed-country α_1 emission factor (see Table 3). Fugitive emissions from feedstock uses are generally expected to be lower than those from production (TEAP, 2022). We assumed a fixed feedstock emission factor of $\alpha_2 = 0.1$ %, representing the "low" estimate reported by TEAP (2022). Note, where consumption is negative (i.e. exports exceed production plus imports), we assume no feedstock use emission. Similarly, we adopt a fixed supply chain emissions factor of $\alpha_3 = 0.1$ %, representing the low estimate for distribution emissions reported by TEAP (2022). The resulting estimated range of total fugitive emissions was 146–594 Gg yr^{-1} in 2020 (Table 3).

Many modern DCE-producing plants are integrated on-site with VCM/PVC production (Cherrie et al., 2011). If the processes are seamless, the distinction between fugitive losses from production and fugitive losses from feedstock use may be less clear-cut compared with other gases. Thus, an alternative framework (not adopted) might be to consider a single emission factor, applied to production, that encapsulates all possible leakage over DCE's internal lifetime within a plant. As we elected to consider global trade and, hence, use consumption in conjunction with production, it was necessary to treat the two terms separately. We note that our overarching goal is to examine the impact of DCE on stratospheric ozone using a global model calibrated to reproduce tropospheric observations of DCE. The overall magnitude and location of DCE emissions is thus important, but the detail of the fugitive source is secondary.

For inclusion in the CTM, the calculated biennial DCE emissions (Table 3) were linearly interpolated to give annual records over the 19-year study period (2002–2020). The emissions were aggregated onto a global 0.5° × 0.5° grid using the country mask of Perrette (2023). This mask was developed for the Inter-Sectoral Impact Model Intercomparison Project (ISIMIP). The within-country DCE distribution was assumed to follow that of ethene. The reaction of ethene with chlorine is the main route by which industrial DCE production occurs; thus, ethene should be a reasonable proxy. Anthropogenic ethene emissions (year 2014) from the "industrial combustion and processes" sector were taken from the gridded (0.5° × 0.5°) datasets produced for CMIP6 (Feng et al., 2020). Figure 2 illustrates the resulting surface DCE emission distribution and time series of regional and global emissions for "scenario sc05", i.e. with $\alpha_1 = 0.5$ % (non-A5)/1.5 %(A5). In this example case, Asia (sum of regions 3–5) accounts for ~48 % of global emissions in 2020. For other Cl-VSLSs, Asian emissions have been assessed to dominate the global anthropogenic source, such as the estimated ~90 % contribution of Asia to global CH$_2$Cl$_2$ emissions reported by Claxton et al. (2020). For DCE, the approach and information described above give rise to a more even distribution of emissions between continents, including a sizeable source outside of Asia.

2.3 CTM and experiments

The temporally varying DCE emissions described in Sect. 2.2 were included in the TOMCAT/SLIMCAT 3-D CTM (Chipperfield, 2006). The model is well evaluated and has been widely used to study the atmospheric budget and impacts of a range of trace gases, including VSLSs (e.g. Claxton et al., 2020; Hossaini et al., 2019). The offline model (hereafter "TOMCAT") is forced by meteorological fields

Table 2. The same as Table 1 but for consumption.

R no.	Region name	2002	2004	2006	2008	2010	2012	2014	2016	2018	2020
1	US/Canada	13 024	13 503	12 827	11 826	12 103	12 744	12 955	14 867	16 882	15 252
2	Europe	10 980	11 632	11 975	11 114	11 354	11 463	11 539	11 503	11 646	11 327
3	S Asia	579	526	540	569	798	1016	993	1066	1307	1186
4	E Asia	10 718	11 510	11 920	11 712	11 836	11 373	11 960	12 935	14 642	14 595
5	SE Asia	1365	1423	1498	1742	1848	1967	1834	2339	2492	2545
6	Australia/NZ	< 1	< 1	< 1	< 1	< 1	< 1	< 1	< 1	< 1	< 1
7	Africa, north	118	145	145	140	147	260	448	482	536	1011
8	Africa, sub-Saharan	202	175	208	152	264	224	264	281	264	240
9	Middle East	1095	1234	1458	1264	1990	2265	2386	2627	2614	2603
10	Central America	390	284	535	568	662	631	610	91	106	90
11	South America	1036	1008	1223	1580	1395	1415	1563	1610	1479	1403
12	E Europe/N Asia	944	938	1288	1246	1210	1034	1179	1360	1820	1890
13	Central Asia.	< 1	< 1	< 1	< 1	< 1	< 1	< 1	< 1	< 1	< 1
	Global total	40 457	42 384	43 623	41 882	43 611	44 398	45 737	49 164	53 792	52 146

Table 3. Estimated global DCE emissions (Gg) due to fugitive losses between 2002 and 2020 (assuming 100 % of DCE consumption is for feedstock use) and for different assumed production emission factors (α_1) in non-A5 (developed) and A5 (developing) countries.

Scenario	α_1 (%)		Global DCE emission (Gg yr^{-1})									
	Non-A5	A5	2002	2004	2006	2008	2010	2012	2014	2016	2018	2020
sc01	0.1	0.3	105	111	116	114	120	123	127	136	150	146
sc02	0.2	0.6	166	175	185	183	193	199	204	218	241	236
sc03	0.3	0.9	227	239	254	251	266	274	282	301	333	325
sc04	0.4	1.2	288	304	323	320	339	349	359	384	425	415
sc05	0.5	1.5	349	368	392	389	412	425	437	467	516	505
sc06	0.6	1.8	410	433	461	458	485	500	515	549	608	594

from the European Centre for Medium-Range Weather Forecasts (ECMWF) ERA5 dataset (Hersbach et al., 2020). The model uses the Prather (1986) scheme for tracer advection and the Holtslag and Boville (1993) scheme to represent boundary layer mixing. For convective transport, the model here utilized archived convective mass fluxes from ERA5. This approach was previously evaluated for ERA-Interim by Feng et al. (2011) and found to perform well. All simulations were performed at a $2.8° \times 2.8°$ (T42 Gaussian grid) horizontal resolution and with 60 hybrid sigma-pressure (σ-p) levels extending from the surface to ~ 60 km.

To test model–measurement agreement under different DCE scenarios and, thus, provide constraint on the global DCE source strength, a reduced chemistry configuration of the CTM was used. In this configuration, the concentration of the hydroxyl radical (OH) was prescribed from the monthly varying climatology produced for the Atmospheric Tracer Transport Model Intercomparison Project (TransCom) on methane (Patra et al., 2011). Six simulations were performed in which the model DCE tracer was controlled by differing surface emissions (Table 3), along with transport, and oxidation by OH. The rate constant for the DCE + OH reaction (k_{OH}) was specified from the latest Jet Propulsion Lab-

oratory (JPL) kinetics evaluation (Burkholder et al., 2020): $k_{OH} = 1.14 \times 10^{-11} \exp(-1150/T)$. The reaction was assumed to proceed as follows: DCE + OH $\rightarrow$ 2Cl + products. There is no current recommendation given for DCE absorption cross sections and, like other chlorinated VSLSs, photolysis is expected to be a minor tropospheric sink (Carpenter et al., 2014) and so was not considered. Deposition was not included as a DCE sink but is expected to be relatively minor.

To diagnose DCE's contribution to stratospheric chlorine and its effect on ozone, we used a CTM configuration with "full" stratospheric chemistry. This configuration includes a treatment of all major processes that control polar and extrapolar ozone (e.g. Chipperfield et al., 2018). Full-chemistry simulations considered only the most likely range of DCE emissions (determined in Sect. 3.1), and the DCE tracer was treated as described above. In the troposphere, chlorine atoms released from DCE oxidation will quickly speciate into HCl, the dominant inorganic chlorine (Cl_y) reservoir (e.g. via $CH_4 + Cl \rightarrow HCl + products$). Tropospheric removal of HCl and other Cl_y species (HCl, HOCl, and $ClONO_2$) via wet and dry deposition was calculated with the standard tropospheric TOMCAT routines (Giannakopoulos et al., 1999; Monks et al., 2017). Henry's law data used to cal-
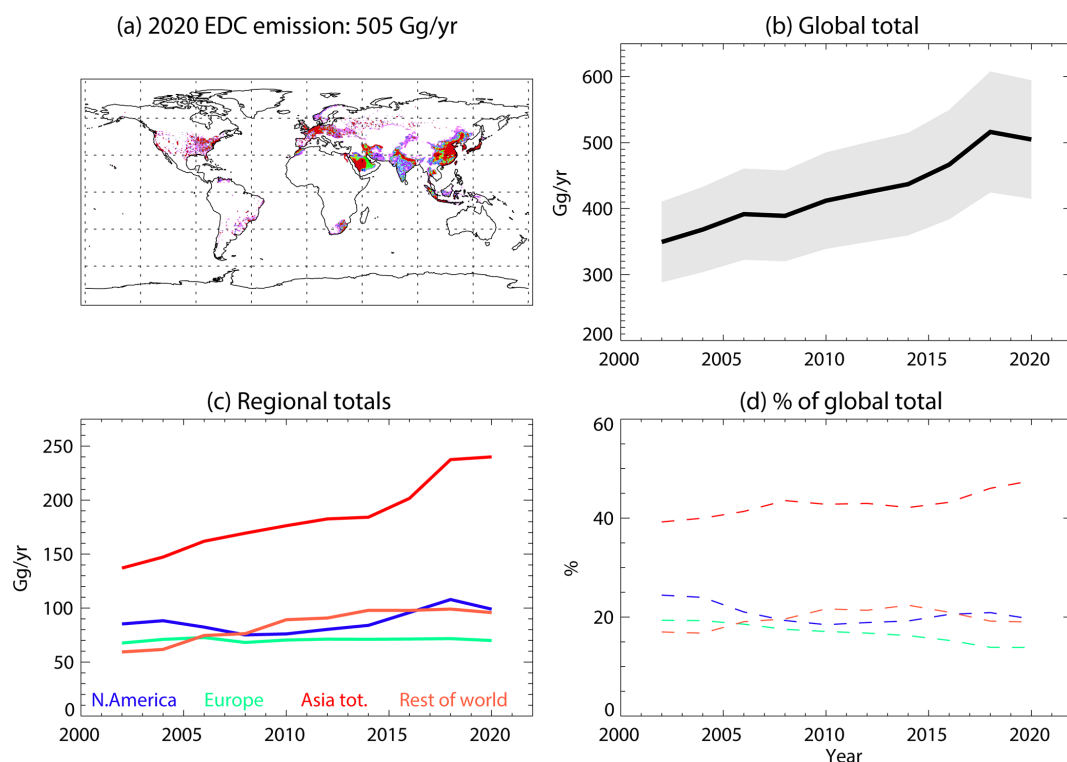
Figure 2. (a) Estimated global surface DCE emission distribution in January 2020 (10^{-2} kg m^{-2} s^{-1}). **(b)** Global total DCE emission vs. year (Gg yr^{-1}). **(c)** Regional total DCE emissions vs. year. **(d)** Proportion of global DCE emissions by region (%). All data are based on scenario sc05 (i.e. assuming $\alpha_1 = 0.5\%$ or 1.5%), with the lower and upper uncertainty (grey shading) in panel **(b)** denoting the sc04 and sc06 cases, respectively.

culate wet deposition rates were taken from Sander (2023). Full-chemistry model runs were spun up for 10 years and then run over the full 19-year analysis period (2002–2020). The stratospheric chlorine and ozone responses to DCE emissions were diagnosed from paired simulations (i.e. comparing runs with DCE emissions to a no-DCE control run). Temporally varying surface mixing ratios of long-lived gases (e.g. halogenated ODSs, N₂O, and CH₄) were prescribed from the data given in WMO (2018).

2.4 DCE observations

We have utilized a range of aircraft measurements of DCE to evaluate the model and to provide constraints on the global DCE source strength. The HIAPER Pole-to-Pole Observations (HIPPO) mission (e.g. Wofsy et al., 2011) was conducted between 2009 and 2011 and involved measurements of a wide range of trace gases predominately over the Pacific from aboard the National Science Foundation (NSF) Gulfstream V aircraft. Sampling extended over a large latitude range from roughly the North Pole to the Antarctic Ocean and from the surface to ∼14 km. The mission comprised five campaigns conducted in different seasons: HIPPO-1 (January 2009), HIPPO-2 (November 2009), HIPPO-3 (March–April 2010), HIPPO-4 (June 2011), and HIPPO-5 (August–

September 2011). Measurements of DCE were obtained by the University of Miami based on the analysis of whole air samples collected in flask samples during each campaign.

The more recent NASA Atmospheric Tomography (ATom) mission was conducted between 2016 and 2018 and also involved extensive measurements of trace gases over a wide latitude range spanning both hemispheres (near pole to pole), including over the Pacific and the Atlantic. Measurements were obtained up to an altitude of ∼12 km aboard the NASA DC-8 aircraft over four campaigns covering different seasons: ATom-1 (July–August 2016), ATom-2 (January–February 2017), ATom-3 (September–October 2017), and ATom-4 (April–May 2018). An overview of the ATom mission, including some scientific highlights, is given in Thompson et al. (2022). For this study, we have used DCE measurements obtained by NOAA from air samples collected with the Programmable Flask Package (PFP) whole air sampler. The DCE measurement precision is around 1% on average (for mole fractions of 1–2 ppt), and the detection limit is < 1 ppt. Regarding sample stability, NOAA ATom sampling was conducted via pressurization into glass flasks; note that there has been no indication of systematic growth or destruction of DCE in glass flasks over time within the measurement precision. Like HIPPO, the spatial coverage of ATom makes it an especially useful dataset with which

Table 4. Observed (Obs.) and modelled (Model) mean DCE abundance (ppt) in the boundary layer (< 3 km) and in different latitude bins during HIPPO and ATom. n denotes the number of measurements in each bin. Mean DCE is reported with ± 1 SD. The mean bias (MB, model minus observation) is given for each bin. Model results are based on DCE emission scenario sc05.

Latitude bin	HIPPO campaign				ATom campaign			
	n	Obs.	Model	MB	n	Obs.	Model	MB
$> 80° $N	11	13.3 (± 4.5)	12.6 (± 4.7)	-0.7	2	17.7 (± 2.6)	20.3 (± 3.0)	2.6
60–80° N	77	14.8 (± 4.5)	12.5 (± 4.5)	-2.3	40	16.4 (± 3.5)	19.3 (± 4.0)	2.9
40–60° N	67	15.2 (± 4.2)	13.0 (± 4.7)	-2.2	55	17.3 (± 5.9)	18.6 (± 4.4)	1.3
20–40° N	53	15.9 (± 6.7)	11.1 (± 4.8)	4.8	28	16.4 (± 8.3)	17.0 (± 6.4)	0.7
0–20° N	49	8.5 (± 3.7)	6.0 (± 3.1)	-2.5	42	8.9 (± 5.1)	7.5 (± 4.2)	-1.3
0–20° S	40	3.5 (± 1.2)	2.3 (± 0.9)	-1.2	25	3.5 (± 1.2)	2.7 (± 0.7)	-0.7
20–40° S	68	1.9 (± 0.5)	1.9 (± 0.6)	0.02	21	1.9 (± 0.3)	2.2 (± 1.1)	0.3
40–60° S	36	1.9 (± 0.4)	2.1 (± 0.6)	0.2	35	1.8 (± 0.3)	2.1 (± 0.6)	0.4
$> 60° $S	12	1.8 (± 0.4)	2.0 (± 0.6)	0.2	22	1.7 (± 0.2)	2.1 (± 0.5)	0.4

to evaluate global models (e.g. the representation of hemispheric gradients). In our subsequent analysis, data from both HIPPO and ATom have been aggregated into nine latitude bins ($> 80°$ N, 60–80° N, 40–60° N, 20–40° N, 0–20° N, 0–20° S, 20–40° S, 40–60° S, and $< 60°$ S). The mean, standard deviation, and number of data points for each bin (boundary layer only, < 3 km) are given in Table 4.

To examine model performance over Asia, we also used measurements obtained during the 2016 Korea–United States Air Quality Study (KORUS-AQ) mission. The mission took place in the months of May and June and included 20 research flights of the NASA DC-8 aircraft based from Osan Air Base, approximately 50 km south of Seoul, South Korea (Crawford et al., 2021). Measurements during this campaign targeted local urban sources of photochemical pollutants; therefore, the air sampled differs considerably from that sampled during HIPPO and ATom. Measurements of DCE and other gases were obtained from whole air samples collected by the University of California, Irvine (UCI) from the surface up to an altitude of ~ 11 km. The measurement detection limit was 0.1 pptv, and the measurement precision was 5 % (Simpson et al., 2020). The UCI group has run extensive tests on the stability of compounds in their canisters in the time between sampling and analysis, and DCE is stable within the canisters. Highly elevated levels of DCE and other volatile organic compounds were reported from KORUS-AQ, especially in air masses originating from China (Simpson et al., 2020). For the analysis here, the DCE mole fractions were aggregated into eight altitude bins (0–8 km) of 1 km depth. Sampling was extensive, and the number of measurements in each bin ranged from 94 to 1323.

To further evaluate model performance over eastern Asia, we used surface DCE measurements made by the University of East Anglia (UEA) at Bachok Marine Research Station, which is located in northeast Malaysia (6.009° N, 102.425° E), and at two sites in Taiwan: (1) Fuguei Cape, on the northern Taiwanese coast (25.297° N, 121.538° E), and

(2) Hengchun, on the southern Taiwanese coast (22.0547° N, 120.6995° E). Measurements of DCE and other Cl-VSLSs at each location have been reported by Oram et al. (2017) and show elevated levels with respect to data obtained in other world regions. The same study provides full details of the sampling and instrument method. Briefly, measurements were obtained from whole air samples collected between 2014 and 2020. Sampling is seasonal and primarily targeted at observing emissions from East Asia during the northeast monsoon. Sampling at Bachok occurred in the months of November to March, while sampling at Fuguei Cape (2014 and 2016 onwards) and Hengchun (2013 and 2015 only) mostly occurred in March to May (Table S1 in the Supplement). The latter two sites in Taiwan are combined to give a single time series in our subsequent analysis. UEA samples were collected in silco-treated cylinders (stainless steel with inner surface coated with fused silica, Restek), and no issues with sample loss have been noticed. All collected samples were analysed by gas chromatography–mass spectrometry (GC-MS) at UEA, with a typical precision of 1 %–3 %.

Compared with other Cl-VSLSs, scientific interest in DCE from an ozone depletion perspective is relatively new. As such, an international standard calibration scale has not yet been universally adopted across measuring groups. Historically, the scales among the labs considered in this study have not differed by more than 10 %–30 % for gases similar to DCE. However, in the absence of any formal assessment of calibration scale differences, an informal intercomparison for DCE was performed for this work. Background atmospheric DCE mole fractions from two remote sites (Barrow and Samoa observatories), where both the NOAA and UCI groups sample, were compared (2017–2023). This intercomparison revealed an average offset of up to ~ 30 % (UCI relatively high and NOAA relatively low), i.e. at the upper end of the above range. While this comparison is limited in scope and will require further effort to refine (beyond the scope of

this paper), this uncertainty is highlighted in the ensuing discussion.

3 Results and discussion

3.1 Model–measurement comparison and emission constraint

Observed boundary layer DCE mole fractions (< 3 km), as averages from all deployments of HIPPO (2009–2011) and ATom (2016–2018), are shown in Fig. 3a and b. The measurement data were compiled into nine latitude bins (Sect. 2.4), and the mean (± 1 SD) of each bin is shown. Recall that both missions sampled air in various seasons of the year; thus, the SD variability includes seasonal effects. Measurements from both missions show a strong hemispheric gradient, with mean NH mole fractions of ~ 15 ppt at latitudes greater than $40°$ N and ~ 4 ppt or less in the Southern Hemisphere (SH). For comparison, DCE mole fractions of 7.8 (± 1.5) ppt have previously been reported in background air in the NH based on aircraft measurements from the 2006 NASA INTEX-B mission which sampled around the Gulf of Mexico and over the western Pacific off the coast of the USA (Barletta et al., 2009; Singh et al., 2009). The data in Fig. 3 show that variability is large within the NH, where most DCE production (and emission) is located and where the number of measurements is relatively high. For example, the relative standard deviation of the 20–40° N bin is $\sim 40\%$ (HIPPO) and $\sim 50\%$ (ATom). For comparison, the relative standard deviation in the SH is smaller, e.g. $\sim 21\%$ (HIPPO) and $\sim 12\%$ (ATom) for the $< 60°$ S bin.

Figure 3 also includes the TOMCAT modelled DCE abundance using the different emission scenarios, i.e. assuming different α_1 emission factors (see Sect. 2.2 and Table 3). With scenarios sc01 to sc03, the model exhibits a substantial low bias and is unable to reproduce the magnitude of DCE in either hemisphere or the observed hemispheric gradient from each mission. Better model–measurement agreement for both missions is obtained from runs with scenarios sc04 to sc06, shown by the shaded regions in Fig. 3. The statistics describing model–measurement differences in Table 4 are based on the central sc05 case, i.e. $\alpha_1 = 0.5\%$(non-A5 countries)/1.5%(A5). Under this scenario, the mean bias (model minus observation) varies by latitude and ranges from near zero up to 4.8 ppt. Although underestimating mean DCE observed in the NH during HIPPO, the model falls within the measurement variability, and better agreement is obtained for the comparisons with ATom. Generally, model–measurement biases here are difficult to interpret and could, in part, reflect the model OH field (affecting the DCE lifetime) and/or transport processes; they do not necessarily point to an under- or overestimation of local emissions. Additionally, as for some other VSLSs, differences in calibration scales between measurement groups (recall the discussion in Sect. 2.4) could be a confounding fac-

tor (see also Roozitalab et al., 2024, for a more detailed discussed). Importantly, model–measurement agreement is generally good in the tropics ($\pm 20°$ N/S), the region most relevant for diagnosing transport to the stratosphere, throughout the vertical profile (see Fig. S1 in the Supplement). The low abundance of DCE at SH high latitudes is also well captured.

A comparison of the modelled vertical profile of DCE to that observed during KORUS-AQ (2016) is shown in Fig. 3c. Compared with HIPPO and ATom, far larger observed levels of DCE are apparent at lower altitudes (up to 2.5 ppbv; not shown in Fig. 3c), along with very large variability (see filled grey circles). To accommodate the latter, binned measurement data in Fig. 3c show the median, as opposed to the mean, and the horizontal axis is capped at 80 ppt. (Note that a version of the aforementioned comparison but with the means is shown in Fig. S2.) The maximum observed value of > 2.5 ppb occurred in the 0–1 km bin for air originating from China. A similar maximum of > 2.4 ppb was measured in air originating from an industrial facility in South Korea (Simpson et al., 2020), although we note that a global-scale model is not expected to capture these most extreme values, which included targeted source sampling. Although the model (median ~ 53 ppt under scenario sc05) underestimates the observations (median ~ 69 ppt) in the lowest bin (0–1 km), it is evident from comparing Fig. 3c with Fig. 3a and b that the model shows significantly elevated DCE in this region. Elevated emissions over East Asia are also a clear feature in Fig. 2a. Above 1 km, there is very close agreement between the model and measurements using scenario sc05. A full quantitative comparison is given in Table S2. A previous in-depth analysis of the KORUS-AQ data highlighted that DCE was especially elevated in air originating from China (Simpson et al., 2020). Similarly, during the 2006 NASA INTEX-B mission, analysis of air sampled in polluted plumes from Asia (although especially China) revealed substantially elevated DCE relative to background air and to plumes from the USA (Barletta et al., 2009). Indeed, DCE was used as a tracer of air from China during both INTEX-B and KORUS-AQ.

The modelled DCE abundance is compared to the available surface measurements from Bachok and Taiwan in Fig. 4. As above, the measurements are characterized by large variability, with DCE exceeding 150 ppt at Bachok and 300 ppt at Taiwan on some days. While the model is not expected to capture the most extreme values, the central tendency of the observations appears to be reasonably well captured at both sites under scenario sc05 (see Table S1). Both the measurements and model show especially elevated levels of DCE at Taiwan (median values > 50 ppt in each year of sampling) with respect to levels observed during HIPPO and ATom, suggesting strong regional or local sources and sampling of relatively polluted air in both the Bachok and Taiwanese samples. Samples collected at Bachok, where the model captures the shape of the seasonal cycle well, predominately occur when the site experiences northeasterly winds,
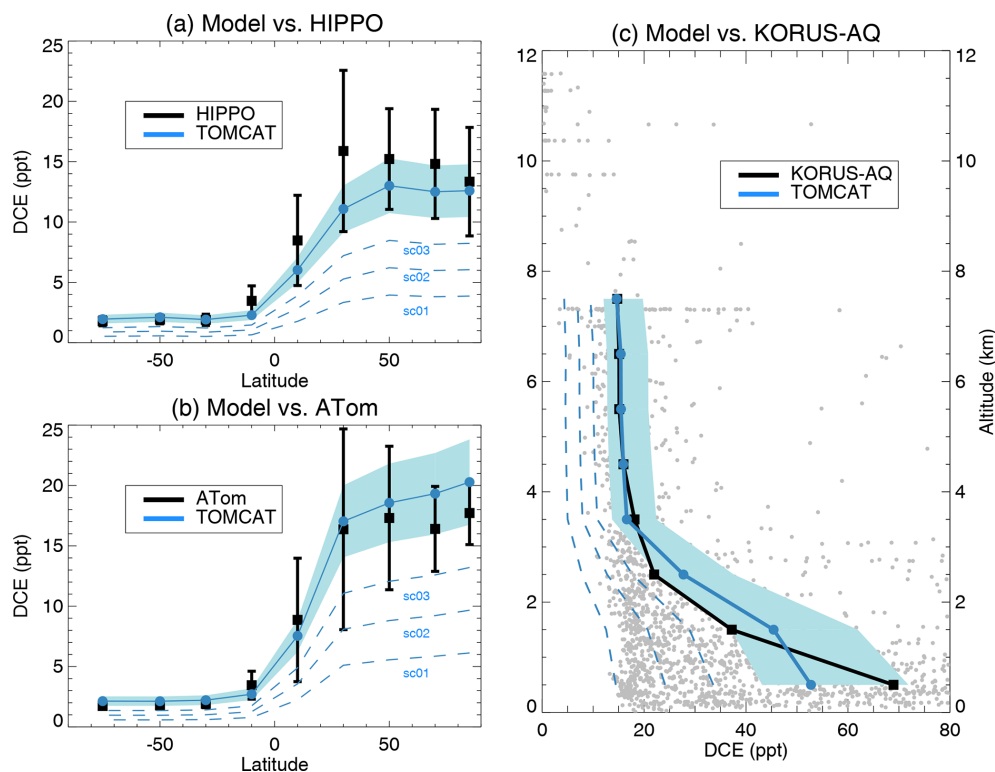
Figure 3. (a, b) Observed DCE mole fractions (ppt) as a function of latitude averaged over all deployments of each HIPPO (2009–2011) and ATom campaign (2016–2018). The data were obtained at < 3 km altitude and have been averaged in nine latitude bins (see Sect. 2.4). Filled black symbols represent the mean within each bin (plotted at the central latitude) and error bars denote ± 1 SD. The corresponding modelled DCE abundance from TOMCAT is shown for different assumed emission factors. Dashed lines denote scenarios sc01 to sc03. The blue shaded region denotes the range obtained from sc04 to sc06 with the central sc05 case indicated (solid line). **(c)** Observed DCE mole fractions vs. altitude from the 2016 KORUS-AQ mission. All data from all flights (filled grey circles) were aggregated into eight altitude bins (see Sect. 2.4) with the median of each bin shown (solid black line). Data points extend to 2.5 ppb but have been cut off at 80 ppt. The corresponding DCE abundance from TOMCAT (also median) is shown, as for other panels.

and observations are thus likely impacted by emissions occurring from mainland China (Oram et al., 2017). This seasonality is discussed in, for example, Oram et al. (2017) and has a large dynamical component. Briefly, strong northeasterly (NE) winds that form in the NH winter transport polluted air masses from continental East Asia deep into the tropics. The prevailing NE winds may also be strengthened during "cold-surge" events. The effect of such events on various tracers have been observed, including at other sites in Malaysia (e.g. Ashfold et al., 2015, 2017). Similarly, owing to close proximity, measurements at Taiwan are expected to be influenced by emissions from mainland China. Although not exhaustive, the comparisons discussed above (along with those for KORUS-AQ) suggest that the model has a reasonable representation of regional emissions in East and Southeast Asia. Note that the modelled DCE abundance at Taiwan (only) was found to exhibit a strong sensitivity to the choice of model vertical level sampled. Therefore, model data in Fig. 4b represent the average of the two model levels closest to the surface.

Although the regional variability in atmospheric DCE measurements can be large, the remote atmospheric survey sampling represented by the HIPPO and ATom missions, along with the other comparisons, allows for some constraint on the global DCE source (given our assumptions concerning the DCE emission distribution). Assuming scenario sc05, $\alpha_1 = 0.5\,\%$ (non-A5 countries)/$1.5\,\%$ (A5 countries), shown above to provide reasonable model–measurement agreement, we estimate a global DCE source of 349 (± 61) Gg yr^{-1} in 2002, rising to 505 (± 90) Gg yr^{-1} in 2020 (i.e. an increase of $\sim 45\,\%$). The mean growth rate of global DCE emissions over this period is ~ 9.1 Gg yr^{-2}. There are very few estimates of global or regional DCE emissions in the literature with which to compare these findings. Using a simple tracer ratio method, Wang et al. (2014) estimated Chinese DCE emissions of 121.6 (± 89) Gg yr^{-1} in 2010. For the same year and again utilizing scenario sc05 (range from sc04 to sc06), our inventory produces significantly lower Chinese DCE emissions of ~ 44 (36–52) Gg yr^{-1}. Oram et al. (2017) estimated Chinese DCE emissions of 203 (± 9) Gg yr^{-1} for 2015 based on measurements obtained in Taiwan and Malaysia.
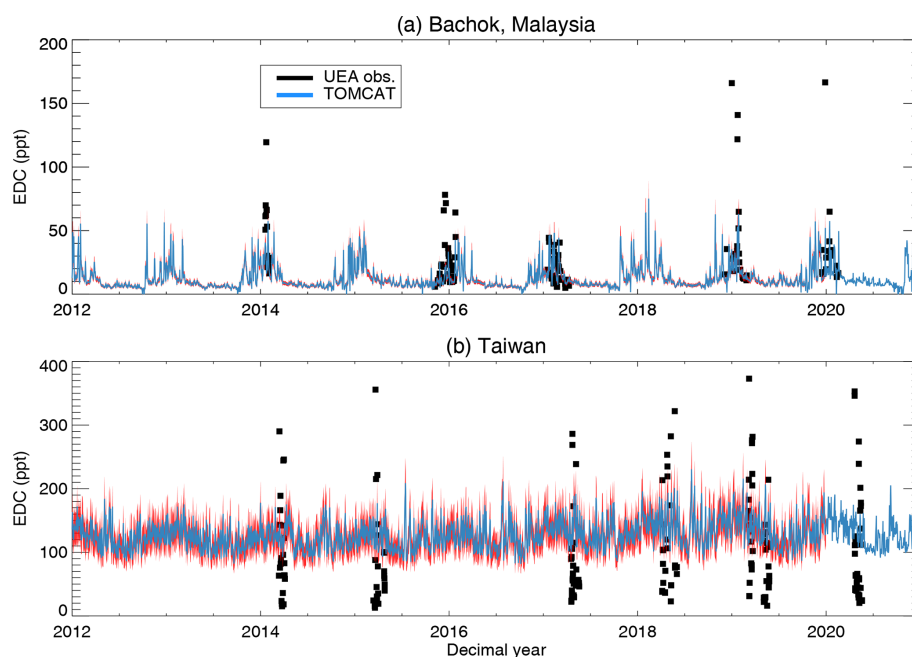
Figure 4. Observed DCE surface mole fraction (ppt) at **(a)** Bachok and **(b)** Taiwan. The corresponding modelled DCE abundance from TOMCAT (sampled daily) is shown for scenario sc05, with the range from scenarios sc04 and sc06 shown in red for clarity.

Our estimate for Chinese emissions in 2016 is ~ 60 (49–71) $\mathrm{Gg\,yr^{-1}}$ and is, thus, substantially lower. However, it should be emphasized that inferred emissions from observed tracer correlations, as in the above studies, are based on several assumptions and subject to large uncertainty. For instance, emissions occurring in nearby regions may confound geographical attribution. Although still lower, our inventory provides better agreement with the above estimates if emissions from, for instance, nearby Taiwan are included. We estimate the sum of DCE emissions from China and Taiwan to be 89 (73–106) Gg in 2010 and 107 (87–127) Gg in 2016. A summary of these comparisons of Chinese emissions is given in Table S3. Further factors that may confound the comparison of these different estimates are the month of measurement and the sampling frequency used to infer tracer ratios. For example, note that the DCE measurements at Bachok reported by Oram et al. (2017), an extended time series of which is shown in Fig. 4a, focus on non-summer months when DCE is relatively abundant at that site.

While the above results provide some constraint on the global DCE source required to reproduce atmospheric observations, some care is needed when interpreting the findings from an emission process standpoint. Our analysis has approximated fugitive emissions arising from production and feedstock use and distribution, assuming that feedstock use accounts for all consumption in every country. However, DCE has known solvent uses (not explicitly accounted for) which may be up to 100 % emissive in the absence of solvent capture and careful disposal. If a non-negligible amount of the observed atmospheric abundance of DCE stems from

solvent use, the contribution from fugitive losses could be overestimated. We anticipate that DCE solvent use is most prevalent in developing countries, where it is relatively cheap vs. alternatives and is readily available and where concerns over its toxicity may not yet have resulted in restrictions on its use. Given these uncertainties, we do not overinterpret our findings from an emission process or sectoral standpoint but rather, with more confidence, highlight the overall magnitude of emissions that provide good agreement with the available measurement data in Fig. 3. In subsequent sections, we present all model quantities assuming scenario sc05 emissions, with reported uncertainties from the sc04 and sc06 cases.

3.2 Lifetime, tropospheric distribution, and contribution to stratospheric chlorine

The modelled tropospheric distribution of DCE is shown in Fig. 5 for the years 2002 and 2020. At the surface (Fig. 5a and b) DCE exhibits large spatial variability and has a strong hemispheric gradient. Hotspots occur within the industrialized zones of its main source regions (USA, Europe, and East Asia). Recall that the DCE emission distribution within countries is prescribed here to follow that of ethene. In reality, the DCE source may be less dispersed than assumed, particularly if fugitive emissions occur from a relatively small number of point plant locations. Growth of DCE in the NH background is apparent from Fig. 5, and we estimate that the global DCE burden increased from ~ 81 (± 15) to ~ 116 (± 21) Gg between 2002 and 2020 (Table 5). Chemical loss

Table 5. Modelled DCE burden (total mass); global loss rate (due to OH); overall global lifetime (burden/loss rate); and contribution to stratospheric chlorine (pptCl) through SGI, PGI, and total (SGI + PGI). All fields are annual averages for the years 2002 or 2020, and results are shown for emission scenarios (sc) sc04, sc05, and sc06.

Scenario	Burden (Gg)		Loss rate (Gg yr⁻¹)		Lifetime (days)		SGI (ppt Cl)		PGI (ppt Cl)		Total Cl (ppt Cl)	
	2002	2020	2002	2020	2002	2020	2002	2020	2002	2020	2002	2020
sc04	67	95	289	417	85	83	5.5	8.8	1.2	1.8	6.7	10.6
sc05	81	116	350	508	85	83	6.7	10.7	1.5	2.2	8.2	12.9
sc06	96	137	411	598	85	83	7.9	12.7	1.7	2.6	9.6	15.3

of DCE is controlled primarily through reaction with OH, and we calculate an overall global DCE lifetime, defined as the ratio of its global burden over its global loss rate, of ∼ 83 d in 2020 (Table 5). This is in very close agreement with the ∼ 82 d reported by Burkholder and Hodnebrog (2022).

It is well established that VSLSs may contribute to stratospheric halogen loading via both source gas injection (SGI) and product gas injection (PGI). Chlorine SGI and PGI from DCE are also shown in Fig. 5. Defining these quantities at the tropical tropopause (∼ 17 km), the total (SGI + PGI) stratospheric chlorine input from DCE in the year 2020 is estimated to be 12.9 (± 2.4) pptCl, comprising 10.7 (± 2) pptCl from SGI and 2.2 (± 0.4) pptCl from PGI (Table 5). For context, the total Cl-VSLS supply to the stratosphere (including VSLSs other than DCE) was estimated to be ∼ 130 (100–160) pptCl in 2019 when total stratospheric chlorine (i.e. including long-lived gases) was around 3240 pptCl (Laube and Tegtmeier et al., 2022). Our DCE SGI estimate in 2020 is similar to the 8.5 (± 1.9) pptCl reported in our previous modelling work (that did not include geographically or temporally varying emissions) for the year 2017 (Hossaini et al., 2019). A notable difference with our previous work is that we assess here that stratospheric chlorine from DCE has increased significantly over time (see Fig. S3), reflecting growth in emissions and hence SGI. Based on an ordinary least-squares regression applied to the model output over the full study period (2002 to 2020; Fig. S3), mean growth rates for SGI and PGI are 0.19 and 0.04 pptCl yr⁻¹, respectively.

In the current study, our estimated chlorine PGI is also similar to the value of ∼ 2 pptCl reported in Hossaini et al. (2019). The latter assumed a fixed lifetime of Cl$_y$ in the troposphere against deposition (∼ 5 d), whereas we adopted an improved, more explicit representation here in which Cl$_y$ washout was calculated using the standard TOMCAT deposition routines for the component chlorine species (Sect. 2.3). As for all VSLSs, lack of observational constraint means that modelled PGI estimates carry significant uncertainty. A process not considered here is the heterogeneous recycling of Cl$_y$ on ice crystals in the upper troposphere, for which there is some observational evidence (von Hobe et al., 2011). As demonstrated for iodine (Saiz-Lopez et al., 2015), such a process could plausibly extend the Cl$_y$ lifetime and thus

increase the magnitude of PGI. However, note that the net effect on PGI will likely depend on the interplay between ice uptake followed by sedimentation and also heterogeneous ice-recycling reactions that return species back to the gas phase (e.g. Fernandez et al., 2014, 2021). Such processes and the required parameters with which to treat them in a global model are highly uncertain.

The model estimates of chlorine SGI from DCE that are presented in Fig. 5c and d and Table 5 are annual mean quantities at the tropical tropopause, averaged zonally over the whole of the tropics (± 20° N/S). While transport across the tropical tropopause is the main route via which air enters the stratosphere, relatively elevated levels of VSLSs (and other gases) have been reported in the subtropical NH lower stratosphere owing to the effects of the Asian summer monsoon (ASM) and ASM anticyclone (e.g. Fiehn et al., 2017; Keber et al., 2020; Lauther et al., 2022). Forming in boreal summer, ASM dynamics are characterized by a rapid uplift of boundary layer air to the upper troposphere and lower stratosphere by deep convection (e.g. Randel and Park, 2006; Basha et al., 2020), including relatively polluted air masses from South and East Asia (e.g. Li et al., 2005; Randel et al., 2010; Müller et al., 2016). Based on aircraft measurements obtained during the Asian Monsoon Anticyclone 2017 campaign (AMA-17) over the Indian subcontinent, Adcock et al. (2021) reported a mean DCE mole fraction around the tropopause (355–375 K) of ∼ 12 ppt (with a range of 4.5 to 23 ppt), corresponding to a chlorine SGI (i.e. 2× the DCE mole fraction) in the range of 9–47 pptCl. The AMA-17 measurements were obtained in July and August in the latitude range of 21–29° N, longitude range of 79–91° E, and from an altitude of ∼ 10–20 km. The measurements from Adcock et al. (2021) are shown in Fig. S4 along with corresponding model estimates. There is generally good agreement between the two datasets, and the model corroborates the signal of relatively large levels of DCE around the tropopause (∼ 10 ppt) and hence a larger local stratospheric chlorine SGI (∼ 20 pptCl) in this region/season relative to the annual mean quantities around the tropical tropopause reported in Table 5.

Other recent studies have also highlighted the importance of Asian emissions in contributing to the atmospheric loading of a range of Cl-VSLSs. For example, in a global mod-
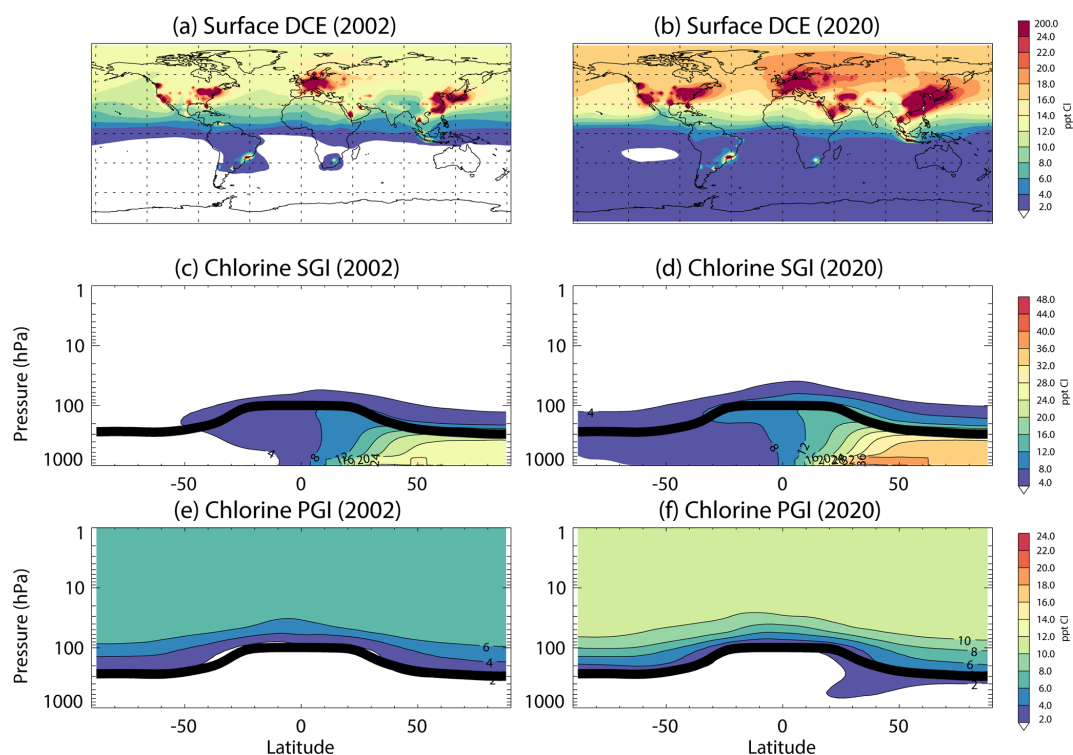
Figure 5. Modelled annual mean DCE volume mixing ratio (ppt) at the surface under scenario sc05 in **(a)** 2002 and **(b)** 2020. Panels **(c)** and **(d)** show the latitude–pressure distribution of chlorine SGI from DCE (ppt Cl) for the same years. Panels **(e)** and **(f)** show chlorine PGI from DCE (ppt Cl). The thermal tropopause pressure based on ERA5 reanalysis (Hoffmann and Spang, 2022) is shown by the black line.

elling study, Roozitalab et al. (2024) used a "tagged tracer" approach to show that Asian emissions likely dominate the global CH_2Cl_2 and C_2Cl_4 distribution. This was the case not only at the surface but also at high altitudes (150 hPa). The same study also analysed measurements of several Cl-VSLSs (including DCE) during the ATom campaign and tentatively assigned relatively enhanced NH mid-latitude mole fractions of Cl-VSLSs (observed during ATom-1) as being influenced by deep convection associated with the Asian summer monsoon. High-altitude aircraft observations from the Asian Summer Monsoon Chemical and Climate Impact Project (ACCLIP) mission have also revealed that the lower stratospheric abundance of Cl-VSLSs above the East Asian monsoon is at least a factor of 2 larger than previously observed in the tropics (Pan et al., 2024).

3.3 Impact of DCE emissions on ozone

The modelled stratospheric ozone change due to DCE under 2020 conditions is shown in Fig. 6. DCE decreases stratospheric ozone globally, although the effect is generally small. The largest absolute decreases occur in the upper stratosphere (10–1 hPa) and polar lower stratosphere (200–20 hPa), i.e. regions where chlorine-catalysed ozone loss is known to be important (e.g. Chipperfield et al., 2018). The absolute ozone decreases in Fig. 6a and b are up to ∼ 5 ppb

when expressed as an annual average (Fig. 6a). Larger decreases (up to ∼ 10 ppb) occur within SH high latitudes in spring when the Antarctic ozone hole forms (Fig. 6b). Corresponding ozone changes (expressed in percent) are shown in Fig. 6c and d. In most regions, the ozone changes due to DCE represent changes of < 1 %, although reductions of up to ∼ 1.3 % in the lower stratosphere are found in the SH polar spring.

The small (although non-zero) effect of DCE on global stratospheric ozone reflects the relatively small input of chlorine from DCE to the stratosphere (see above). However, as noted, several studies have identified transport via the ASM as a route through which relatively large local injections of various VSLSs (including DCE) to the extratropical lower stratosphere can occur (Keber et al., 2020; Adcock et al., 2021; Lauther et al., 2022; Pan et al., 2024). In principle, this process and its effect on chlorine injection from DCE is represented in our model (see Fig. S4). However, the very large surface levels of DCE, in at least some parts of Asia (see Fig. 3c), that are not tightly constrained by the data considered here may be underestimated in this analysis and thus too the co-location of emission hotspots with regions of relatively fast vertical ascent. Nonetheless, the local impact of DCE on summertime stratospheric ozone in the ASM region was briefly examined and is shown in Fig. S5. Noting again that chlorine-catalysed ozone destruction is generally effi-
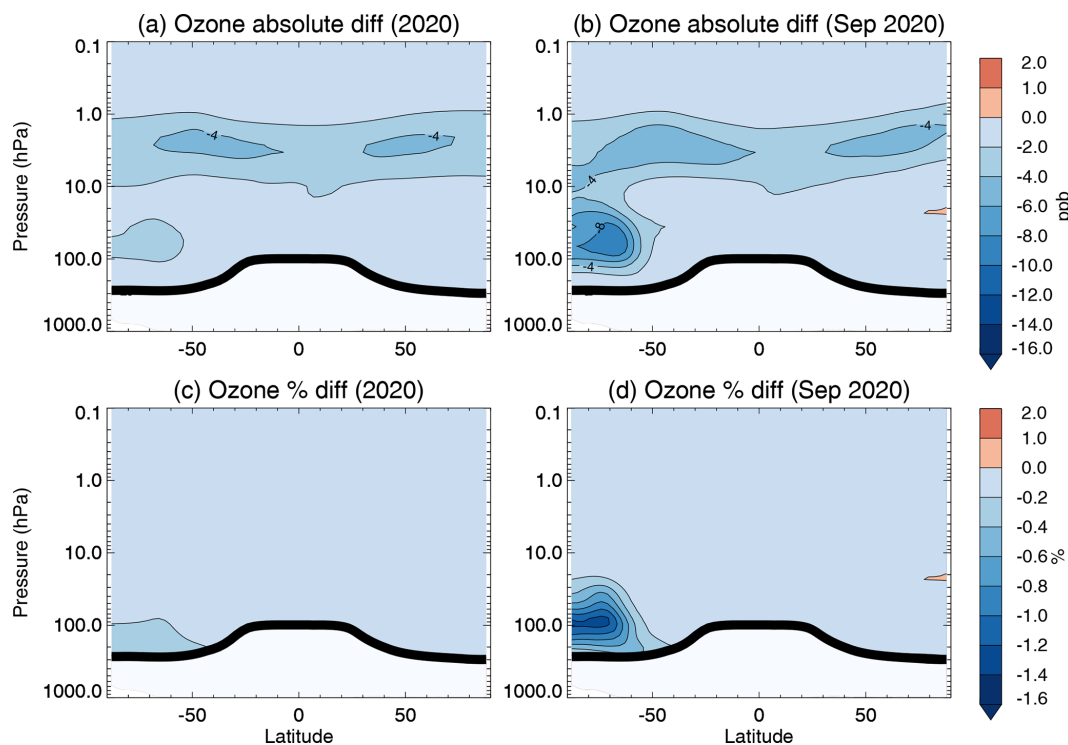
Figure 6. Modelled stratospheric ozone decrease due to DCE in 2020 expressed as **(a, c)** an annual average and **(b, d)** September average (i.e. Antarctic ozone hole season). Panels **(a)** and **(b)** show absolute decreases (ppb), whereas panels **(c)** and **(d)** show percentages. Model results calculated based on the difference between simulations with DCE (scenario sc05) and without DCE.

cient in the polar lower stratosphere and upper stratosphere, we find that ozone changes due to DCE in the lower stratosphere above the ASM region/season (i.e. the localized effect) are small ($< 0.1\%$). Ultimately, the overall significance of the ASM transport pathway for VSLS-driven stratospheric ozone loss is an area of current research that requires further and more detailed investigation considering other VSLS species (including those with predominately natural sources) and would benefit from new measurements in this region.

This study has focussed only on the possible direct impact of DCE emissions on ozone. However, we note that a broader impact assessment (beyond the scope of this work) might also factor in the unintended, although expected to be very minor, formation of other halogenated chemicals that inevitably occur during the DCE production process (the majority of these are destroyed by thermal oxidation or other means). These species are found in the "lights" and "heavies" effluent streams that may range from 0.3 % to 1.0 % of the DCE produced (TEAP, 2022) and include a proportion of ODSs, such as carbon tetrachloride (CCl$_4$), and other chlorinated VSLSs, such as chloroform (CHCl$_3$).

4   Summary and concluding remarks

The global production of DCE in the year 2020 exceeded 50×10^6 t. However, despite the annual production volume

greatly exceeding that of other more prominent industrial VSLSs (e.g. CH$_2$Cl$_2$ and CHCl$_3$), few atmospheric observations of DCE exist and little is known of its global budget. In this study, we combined information on industrial DCE production, trade statistics, and assumptions on its fugitive losses to explore the plausible range of global DCE emissions. Temporally varying gridded DCE emission fields were developed using a bottom-up approach and then included in the TOMCAT CTM. Transient simulations were performed to assess the DCE source required to reproduce a variety of measurements from recent aircraft missions (HIPPO, ATom, and KORUS-AQ) and from ground sites in Southeast Asia. Based on constraints provided by these comparisons, we infer a global DCE source of 349 ($\pm$ 61) Gg yr^{-1} in 2002, rising to 505 ($\pm$ 90) Gg yr^{-1} in 2020 (i.e. an increase of $\sim 45\%$). Our framework for calculating DCE emissions assumed that all releases to the atmosphere result from fugitive losses during its production, its use as a feedstock (largely to produce VCM in the PVC production chain), and during its supply chain. Reasonably good agreement between the model and DCE observations is achieved by assuming a production emission factor of $\sim 0.5\%$ in developed countries and 1.5 % in developing countries. These factors are within the generic "most likely" range of factors (0.9 %–4.0 %) applicable to a range of other gases assessed by TEAP (2022). Large uncertainty around the magnitude and emissions asso-

ciated with DCE solvent use, which is potentially widespread in developing countries and East Asia, is a confounding factor in our analysis and prevents firm conclusions as to the specific sectors contributing to the observed DCE signal and the global distribution of these emissions.

We estimate that DCE contributed 12.9 ($\pm$ 2.4) ppt of chlorine to the stratosphere in 2020. Based on this loading, we estimate that DCE decreased ozone by up to several parts per billion in 2020, with the largest changes occurring in the upper stratosphere and high-latitude lower stratosphere. Outside of the SH lower stratosphere in spring, where the ozone decreases attributable to DCE are up to $\sim$ 1.3 %, the effect of DCE on global stratospheric ozone is presently small ($<$ 1 %), although non-zero. Any future growth in DCE emissions (e.g. tied to downstream demand for PVC) may increase the contribution of DCE to stratospheric chlorine and thereby increase its impact on ozone. Such possible future effects would need to be examined with knowledge of the global PVC market and its possible future trajectories as well as an assessment of use and emissions from the DCE solvent sector. Diagnosing future changes in the contribution of DCE to ozone-depleting chlorine in the stratosphere would also benefit from routine observations of DCE at sites across the globe.

Author contributions. RH conceived and led the study and developed the emission inventories in collaboration with and based on data, analysis, and advice provided by DS. ZW performed the TOMCAT/SLIMCAT model simulations, with supervision from MPC and WF. AM and AL contributed to the analysis of model output. DO, KA, CC, SAM, IJS, and EA provided atmospheric measurements and interpretation of these data. RH prepared the original draft of the paper. All authors contributed to reviewing and editing the manuscript.

References

Adcock, K. E., Fraser, P. J., Hall, B. D., Langenfelds, R. L., Lee, G., Montzka, S. A., Oram, D. E., Röckmann, T., Stroh, F., Sturges, W. T., Vogel, B., and Laube, J. C.: Aircraft-Based Observations of Ozone-Depleting Substances in the Upper Troposphere and Lower Stratosphere in and Above the Asian Summer Monsoon, J. Geophys. Res.-Atmos., 126, e2020JD033137, https://doi.org/10.1029/2020jd033137, 2021.

An, M., Western, L. M, Say, D., Chen, L., Claxton, T., Ganesan, A. L, Hossaini, R., Krummel, P. B, Manning, A. J, Mühle, J., O'Doherty, S., Prinn, R. G, Weiss, R. F, Young, D., Hu, J., Yao, B., and Rigby, R.: Rapid increase in dichloromethane emissions from China inferred through atmospheric observations, Nat. Commun., 12, 7279, https://doi.org/10.1038/s41467-021-27592-y, 2021.

An, M., Western, L. M, Hu, J., Yao., B., Mühle, J., Ganesan, A. L, Prinn, R. G, Krummel, P. B, Hossaini, R., Fang, X., O'Doherty, S., Weiss, R. F, Young, D., and Rigby, M.: Anthropogenic Chloroform Emissions from China Drive Changes in Global Emissions, Environ. Sci. Technol., 57, 13925–13936, https://doi.org/10.1021/acs.est.3c01898, 2023.

Ashfold, M. J., Pyle, J. A., Robinson, A. D., Meneguz, E., Nadzir, M. S. M., Phang, S. M., Samah, A. A., Ong, S., Ung, H. E., Peng, L. K., Yong, S. E., and Harris, N. R. P.: Rapid transport of East Asian pollution to the deep tropics, Atmos. Chem. Phys., 15, 3565–3573, https://doi.org/10.5194/acp-15-3565-2015, 2015.

Ashfold, M. J Latif, M. T, Samah, A. A, Mead, M. I, and Harris, N. RP.: Influence of Northeast Monsoon cold surges on air quality in Southeast Asia, Atmos. Environ., 166, 498–509, https://doi.org/10.1016/j.atmosenv.2017.07.047, 2017.

ATSDR: Toxicological Profile for 1,2-Dichloroethane, Chapter 5 (Potential For Human Exposure), Agency for Toxic Substances and Disease Registry, Atlanta, GA, U.S. Department of Health and Human Services, Public Health Service, https://www.atsdr.cdc.gov/toxprofiles/tp38.pdf (last access: 22 November 2024), 2024.

Ayres, R. U. and Ayres, L. W.: The Life Cycle of Chlorine, Part II: Conversion Processes and Use in the European Chemical Industry, J. Ind. Ecol., 1, 65–89, https://doi.org/10.1162/jiec.1997.1.2.65, 1997.

Basha, G., Ratnam, M. V., and Kishore, P.: Asian summer monsoon anticyclone: trends and variability, Atmos. Chem. Phys., 20, 6789–6801, https://doi.org/10.5194/acp-20-6789-2020, 2020.

Barletta, B., Meinardi, S., Simpson, I. J., Atlas, E. L., Beyersdorf, A. J., Baker, A. K., Blake, N. J., Yang, M., Midyett, J. R., Novak, B. J., McKeachie, R. J., Fuelberg, H. E., Sachse, G. W., Avery, M. A., Campos, T., Weinheimer, A. J., Rowland, F. S., and Blake, D. R.: Characterization of volatile organic compounds (VOCs) in Asian and north American pollution plumes during INTEX-B: identification of specific Chinese air mass tracers, Atmos. Chem. Phys., 9, 5371–5388, https://doi.org/10.5194/acp-9-5371-2009, 2009.

Bednarz, E. M., Hossaini, R., Chipperfield, M. P., Abraham, N. L., and Braesicke, P.: Atmospheric impacts of chlorinated very short-lived substances over the recent past – Part 1: Stratospheric chlorine budget and the role of transport, Atmos. Chem. Phys., 22, 10657–10676, https://doi.org/10.5194/acp-22-10657-2022, 2022.

Bednarz, E. M., Hossaini, R., and Chipperfield, M. P.: Atmospheric impacts of chlorinated very short-lived substances over the recent past – Part 2: Impacts on ozone, EGUsphere [preprint], https://doi.org/10.5194/egusphere-2023-496, 2023.

Burkholder, J. B. and Hodnebrog, Ø.: Summary of Abundances, Lifetimes, ODPs, REs, GWPs, and GTPs, in: Scientific assessment of ozone depletion: 2022, GAW Report No. 278, Annex, World Meteorological Organization, Geneva, Switzerland, ISBN 978-9914-733-97-6, 2022.

Burkholder, J. B., Sander, S. P., Abbatt, J., Barker, J. R., Cappa, C., Crounse, J. D., Dibble, T. S.and Huie, R. E., Kolb, C. E., Kurylo, M. J., Orkin, V. L., Percival, C. J., Wilmouth, D. M., and Wine, P. H.: Chemical Kinetics and Photochemical Data for Use in Atmospheric Studies, Evaluation No. 19, Tech. rep., JPL Publication 19-5, Jet Propulsion Laboratory, Pasadena, https://jpldataeval.jpl.nasa.gov/ (last access: 22 November 2024), 2020.

Carpenter, L. J., Reimann, S., Burkholder, J. B., Clerbaux, C., Hall, B. D., Hossaini, R., Laube, J. C., and Yvon-Lewis, S. S.: Update on ozone-depleting substances (ODSs) and other gases of interest to the Montreal Protocol, in: Scientific assessment of ozone depletion: 2014, Global Ozone Research and Monitoring Project Report No. 55, Chap. 1, World Meteorological Organization, Geneva, Switzerland, ISBN 978-9966-076-01-4, 2014.

CEH: Chemical Economics Handbook, https://www.spglobal.com/commodityinsights/en/ci/products/ethylene-dichloride-chemical-economics-handbook.html (last access: 22 November 2024), 2023.

Cherrie, J. W, Gorman, M., Shafrir, A., van Tongeren, M., Mistry, M., Sobey, M., Corden, C., Rushton, L., and Hutchings, S.: Health, socio-economic and environmental aspects of possible amendments to the EU Directive on the protection of workers from the risks related to exposure to carcinogens and mutagens at work, IOM Research Project, SHEcan Report P937/17, https://ec.europa.eu/social/BlobServlet?docId=10149&langId=en (last access: 22 November 2024), 2011.

Chinabaogao: The current status and development prospects of production and consumption of ethylene dichloride in my country, https://free.chinabaogao.com/huagong/201206/062113C592012.html (last access: 22 November 2024), 2012 (in Chinese).

Chipperfield, M. P.: New version of the TOMCAT/SLIMCAT offline chemical transport model: intercomparison of stratospheric tracer experiments, Q. J. Roy. Meteor. Soc., 132, 1179–1203, https://doi.org/10.1256/qj.05.51, 2006.

Chipperfield, M. P., Dhomse, S., Hossaini, R., Feng, W., Santee, M. L., Weber, M., Burrows, J. P., Wild, J. D., Loyola, D., and Coldewey-Egbers, M.: On the cause of recent variations in lower stratospheric ozone, Geophys. Res. Lett., 45, 5718–5726, https://doi.org/10.1029/2018GL078071, 2018.

Claxton, T., Hossaini, R., Wild, O., Chipperfield, M. P., and Wilson, C.: On the regional and seasonal ozone depletion potential of chlorinated very short-lived substances, Geophys. Res. Lett., 46, 5489–5498. https://doi.org/10.1029/2018GL081455, 2019.

Claxton, T., Hossaini, R., Wilson, C., Montzka, S. A., Chipperfield, M. P., Wild, O., Bednarz, E. M., Carpenter, L. J., Andrews, S. J., Hackenberg, S. C., Mühle, J., Oram, D., Park, S., Park, M.-K., Atlas, E., Navarro, M., Schauffler, S., Sherry, D., Vollmer, M., Schuck, T., Engel, A., Krummel, P. B., Maione, M., Arduini, J., Saito, T., Yokouchi, Y., O'Doherty, S., Young, D., and Lunder, C.: A synthesis inversion to constrain global emissions of two very short lived chlorocarbons: dichloromethane, and perchloroethylene, J. Geophys. Res.-Atmos., 125, e2019JD031818, https://doi.org/10.1029/2019JD031818, 2020.

Crawford, J. H., Ahn, J.-Y., Al-Saadi, J., Chang, L., Emmons, L. K., Kim, J., Lee, G., Park, J.-H., Park, R. J., Woo, J. H., Song, C.-K., Hong, J.-H., Hong, Y.-D., Lefer, B. L., Lee, M., Lee, T., Kim, S., Min, K.-E., Yum, S. S., Shin, H. J., Kim, Y.-W., Choi, J.-S., Park, J.-S., Szykman, J. J., Long, R. W., Jordan, C. E., Simpson, I. J., Fried, A., Dibb, J. E., Cho, S., and Kim, Y. P.: The Korea–United States Air Quality (KORUS-AQ) field study, Elementa-Sci. Anthrop., 9, 00163, https://doi.org/10.1525/elementa.2020.00163, 2021.

Engel, A., Rigby, M., Burkholder, J. B., Fernandez, R. P., Froidevaux, L., Hall, B. D., Hossaini, R., Saito, T., Vollmer, M. K., and Yao, B.: Update on ozone-depleting substances (ODSs) and

other gases of interest to the Montreal Protocol, in: Scientific assessment of ozone depletion: 2018, Global Ozone Research and Monitoring Project–Report No. 58, Chapter 1, World Meteorological Organization, Geneva, Switzerland, ISBN 978-1-7329317-1-8, 2018.

ECHA: Background document for 1,2-dichloroethane, European Chemicals Agency, https://echa.europa.eu/documents/10162/c667ff11-b443-3d98-daf9-d6d77727bee1 (last access: 22 November 2024), 2012.

EPA: Use Report for 1,2-Dichloroethane, Environmental Protection Agency, https://downloads.regulations.gov/EPA-HQ-OPPT-2018-0427-0030/content.pdf (last access: 22 November 2024), 2020.

Falk, S., Sinnhuber, B.-M., Krysztofiak, G., Jöckel, P., Graf, P., and Lennartz, S. T.: Brominated VSLS and their influence on ozone under a changing climate, Atmos. Chem. Phys., 17, 11313–11329, https://doi.org/10.5194/acp-17-11313-2017, 2017.

Falta, R. W., Bulsara, N., Henderson, J. K., and Mayer, R. A.: Leaded-gasoline additives still contaminate groundwater: Ethylene dibromide and 1,2-dichloroethane persist at high levels despite a phaseout in the late 1980's, but they get little attention, Environ. Sci. Technol., 39, 379A–384A, https://doi.org/10.1021/es053352k, 2005.

Fang, X., Park, S., Saito, T., Tunnicliffe, R., Ganesan, A. L., Rigby, M., Li, S., Yokouchi, Y., Fraser, P. J., Harth, C. M., Krummel, P. B., Mühle, J., O'Doherty, S., Salameh, P. K., Simmonds, P. G., Weiss, R. F., Young, D., Lunt, M. F., Manning, 295 A. J., Gressent, A., and Prinn, R. G.: Rapid increase in ozone-depleting chloroform emissions from China, Nat. Geosci., 12, 89–93, 2019.

Feng, L., Smith, S. J., Braun, C., Crippa, M., Gidden, M. J., Hoesly, R., Klimont, Z., van Marle, M., van den Berg, M., and van der Werf, G. R.: The generation of gridded emissions data for CMIP6, Geosci. Model Dev., 13, 461–482, https://doi.org/10.5194/gmd-13-461-2020, 2020.

Feng, W., Chipperfield, M. P., Dorf, M., Pfeilsticker, K., and Ricaud, P.: Mid-latitude ozone changes: studies with a 3-D CTM forced by ERA-40 analyses, Atmos. Chem. Phys., 7, 2357–2369, https://doi.org/10.5194/acp-7-2357-2007, 2007.

Feng, W., Chipperfield, M. P., Dhomse, S., Monge-Sanz, B. M., Yang, X., Zhang, K., and Ramonet, M.: Evaluation of cloud convection and tracer transport in a three-dimensional chemical transport model, Atmos. Chem. Phys., 11, 5783–5803, https://doi.org/10.5194/acp-11-5783-2011, 2011.

Fernandez, R. P., Salawitch, R. J., Kinnison, D. E., Lamarque, J.-F., and Saiz-Lopez, A.: Bromine partitioning in the tropical tropopause layer: implications for stratospheric injection, Atmos. Chem. Phys., 14, 13391–13410, https://doi.org/10.5194/acp-14-13391-2014, 2014.

Fernandez, R. P., Barrera, J. A., López-Noreña, A. I., Kinnison, D. E., Nicely, J., Salawitch, R. J., Wales, P. A., Toselli, B. M., Tilmes, S., Lamarque, J.-F., Cuevas, C. A., and Saiz-Lopez, A.: Intercomparison between surrogate, explicit and full treatments of VSL bromine chemistry within the CAM-Chem chemistry-climate model, Geophys. Res. Lett., 48, e2020GL091125, https://doi.org/10.1029/2020GL091125, 2021.

Fiehn, A., Quack, B., Hepach, H., Fuhlbrügge, S., Tegtmeier, S., Toohey, M., Atlas, E., and Krüger, K.: Delivery of halogenated very short-lived substances from the west Indian Ocean to the stratosphere during the Asian summer monsoon, Atmos. Chem. Phys., 17, 6723–6741, https://doi.org/10.5194/acp-17-6723-2017, 2017.

Giannakopoulos, C., Chipperfield, M. P., Law, K. S., and Pyle, J. A.: Validation and intercomparison of wet and dry deposition schemes using ²¹⁰Pb in a global three-dimensional off-line chemical transport model, J. Geophys. Res., 104, 23761–23784, https://doi.org/10.1029/1999JD900392, 1999.

Hersbach, H., Bell, B., Berrisford, P., Hirahara, S., Horányi, A., Muñoz-Sabater, J., Nicolas, J., Peubey, C., Radu, R., Schepers, D., Simmons, A., Soci, C., Abdalla, S., Abellan, X., Balsamo, G., Bechtold, P., Biavati, G., Bidlot, J., Bonavita, M., De Chiara, G., Dahlgren, P., Dee, D., Diamantakis, M., Dragani, R., Flemming, J., Forbes, R., Fuentes, M., Geer, A., Haimberger, L., Healy, S., Hogan, R. J., Hólm, E., Janisková, M., Keeley, S., Laloyaux, P., Lopez, P., Lupu, C., Radnoti, G., de Rosnay, P., Rozum, I., Vamborg, F., Villaume, S., and Thépaut, J.-N.: The ERA5 global reanalysis, Q. J. Roy. Meteor. Soc., 146, 1999–315 2049, https://doi.org/10.1002/qj.3803, 2020.

Hoffmann, L. and Spang, R.: An assessment of tropopause characteristics of the ERA5 and ERA-Interim meteorological reanalyses, Atmos. Chem. Phys., 22, 4019–4046, https://doi.org/10.5194/acp-22-4019-2022, 2022.

Holtslag, A. and Boville, B.: Local versus nonlocal boundary-layer diffusion in a global climate model, J. Climate, 6, 1825–1842, 1993.

Hossaini, R.: DCE emissions from 2024 ACP paper [dataset], https://doi.org/10.17635/lancaster/researchdata/690, 2024.

Hossaini, R., Chipperfield, M. P., Montzka, S. A., Leeson, A. A., Dhomse, S., and Pyle, J. A.: The increasing threat to stratospheric ozone from dichloromethane, Nat. Commun., 8, 15962, https://doi.org/10.1038/ncomms15962, 2017.

Hossaini, R., Atlas, E., Dhomse, S. S., Chipperfield, M. P., Bernath, P. F., Fernando, A. M., Mühle, J., Leeson, A. A., Montzka, S. A., Feng, W., Harrison, J. J., Krummel, P., Vollmer, M. K., Reimann, S., O'Doherty, S., Young, D., Maione, M., Arduini, 320 J., and Lunder, C. R.: Recent trends in stratospheric chlorine from very short-lived substances, J. Geophys. Res.-Atmos., 124, 2318–2335, https://doi.org/10.1029/2018JD029400, 2019.

Huang, M., Carmichael, G. R., Pierce, R. B., Jo, D. S., Park, R. J., Flemming, J., Emmons, L. K., Bowman, K. W., Henze, D. K., Davila, Y., Sudo, K., Jonson, J. E., Tronstad Lund, M., Janssens-Maenhout, G., Dentener, F. J., Keating, T. J., Oetjen, H., and Payne, V. H.: Impact of intercontinental pollution transport on North American ozone air pollution: an HTAP phase 2 multi-model study, Atmos. Chem. Phys., 17, 5721–5750, https://doi.org/10.5194/acp-17-5721-2017, 2017.

IPCC/TEAP: Safeguarding the Ozone Layer and the Global Climate System: Special Report of the Intergovernmental Panel on Climate Change, Cambridge University Press, ISBN 92-9169-118-6, 2005.

Jordan, A., Stoy, P., and Sneddon, H. F.: Chlorinated solvents: their advantages, disadvantages, and alternatives in organic and medicinal chemistry, Chem. Rev., 121, 1582–622, https://doi.org/10.1021/acs.chemrev.0c00709, 2020.

Keber, T., Bönisch, H., Hartick, C., Hauck, M., Lefrancois, F., Obersteiner, F., Ringsdorf, A., Schohl, N., Schuck, T., Hossaini, R., Graf, P., Jöckel, P., and Engel, A.: Bromine from short-lived source gases in the extratropical northern hemi-

spheric upper troposphere and lower stratosphere (UTLS), Atmos. Chem. Phys., 20, 4105–4132, https://doi.org/10.5194/acp-20-4105-2020, 2020.

Laube, J. C., Engel, A., Bönisch, H., Möbius, T., Worton, D. R., Sturges, W. T., Grunow, K., and Schmidt, U.: Contribution of very short-lived organic substances to stratospheric chlorine and bromine in the tropics – a case study, Atmos. Chem. Phys., 8, 7325–7334, https://doi.org/10.5194/acp-8-7325-2008, 2008.

Laube, J. C., Tegtmeier, S., Fernandez, R. P. F., Harrison, J., Hu, L., Krummel, P., Mahieu, E., Park, S., and Western, L., Atlas, E., Bernath, P., Cuevas, C. A., Dutton, G., Froidevaux L., Hossaini, R., Keber, T., Koenig, T. K., Montzka, S. A., Mühle, J., O'Doherty, S., Oram, D. E., Pfeilsticker, K., Prignon, M., Quack, B., Rigby, M., Rotermund, M., Saito, T., Simpson, I. J, Smale, D., Vollmer, M. K., and Young, D.: Update on ozone-depleting substances (ODSs) and other gases of interest to the Montreal Protocol, in: Scientific assessment of ozone depletion: 2022, GAW Report No. 278, Chap. 1, World Meteorological Organization, Geneva, Switzerland, ISBN 978-9914-733-97-6, 2022.

Lauther, V., Vogel, B., Wintel, J., Rau, A., Hoor, P., Bense, V., Müller, R., and Volk, C. M.: In situ observations of CH$_2$Cl$_2$ and CHCl$_3$ show efficient transport pathways for very short-lived species into the lower stratosphere via the Asian and the North American summer monsoon, Atmos. Chem. Phys., 22, 2049–2077, https://doi.org/10.5194/acp-22-2049-2022, 2022.

Li, Q., Jiang, J. H., Wu, D. L., Read, W. G., Livesey, N. J., Waters, J. W., Zhang, Y., Wang, B., Filipiak, M. J., Davis, C. P., Turquety, S., Wu, S., Park, R. J., Yantosca, R. M., and Jacob, D. J.: Convective outflow of South Asian pollution: a global CTM simulation compared with EOS MLS observations, Geophys. Res. Lett., 32, L14826, https://doi.org/10.1029/2005GL022762, 2005.

Lyu, X., Guo, H., Wang, Y., Zhang, F., Nie, K., Dang, J., Liang, Z., Dong, S., Zeren, Y., Zhou, B., Gao, W., Zhao, S., and Zhang, G.: Hazardous volatile organic compounds in ambient air of China, Chemosphere, 246, 125731, https://doi.org/10.1016/j.chemosphere.2019.125731, 2020.

Monks, S. A., Arnold, S. R., Hollaway, M. J., Pope, R. J., Wilson, C., Feng, W., Emmerson, K. M., Kerridge, B. J., Latter, B. L., Miles, G. M., Siddans, R., and Chipperfield, M. P.: The TOMCAT global chemical transport model v1.6: description of chemical mechanism and model evaluation, Geosci. Model Dev., 10, 3025–3057, https://doi.org/10.5194/gmd-10-3025-2017, 2017.

Müller, S., Hoor, P., Bozem, H., Gute, E., Vogel, B., Zahn, A., Bönisch, H., Keber, T., Krämer, M., Rolf, C., Riese, M., Schlager, H., and Engel, A.: Impact of the Asian monsoon on the extratropical lower stratosphere: trace gas observations during TACTS over Europe 2012, Atmos. Chem. Phys., 16, 10573–10589, https://doi.org/10.5194/acp-16-10573-2016, 2016.

NASA: Korea United States Air Quality Study, EarthData [data set], NASA, https://doi.org/10.5067/Suborbital/KORUSAQ/DATA01, 2024.

Oram, D. E., Ashfold, M. J., Laube, J. C., Gooch, L. J., Humphrey, S., Sturges, W. T., Leedham Elvidge, E. C., Forster, G. L., Harris, N. R. P., Mead, M. I., Samah, A. A., Phang, S. M., Ou-Yang, C.-F., Lin, N.-H., Wang, J.-L., Baker, A. K., Brenninkmeijer, C. A. M., and Sherry, D.: A growing threat to the ozone layer from short-lived anthropogenic chlorocarbons, Atmos. Chem. Phys., 17, 11929–11941, https://doi.org/10.5194/acp-17-11929-2017, 2017.

Pan, L. L., Atlas, E. L., Honomichl, S. B., Smith, W. P., Kinnison, D. E., Solomon, S., Santee, M. L., Saiz-Lopez, A., Laube, J. C., Wang, B., Ueyama, R., Bresch, J. F., Hornbrook, R. S., Apel, E. C., Hills, A. J., Treadaway, V., Smith, K., Schauffler, S., Donnelly, S., Hendershot, R., Lueb, R., Campos, T., Viciani, S., D'Amato, F., Bianchini, G., Barucci, M., Podolske, J. R., Iraci, L. T., Gurganus, C., Bui, P., Dean-Day, J. M., Millán, L., Ryoo, J., Barletta, B., Koo, J., Kim, J., Liang, Q., Randel, W. J., Thornberry, T., and Newman, P. A.: East Asian summer monsoon delivers large abundances of very short-lived organic chlorine substances to the lower stratosphere, P. Natl. Acad. Sci. USA, 121, e2318716121, https://doi.org/10.1073/pnas.2318716121, 2024.

Patra, P. K., Houweling, S., Krol, M., Bousquet, P., Belikov, D., Bergmann, D., Bian, H., Cameron-Smith, P., Chipperfield, M. P., Corbin, K., Fortems-Cheiney, A., Fraser, A., Gloor, E., Hess, P., Ito, A., Kawa, S. R., Law, R. M., Loh, Z., Maksyutov, S., Meng, L., Palmer, P. I., Prinn, R. G., Rigby, M., Saito, R., and Wilson, C.: TransCom model simulations of CH$_4$ and related species: linking transport, surface flux and chemical loss with CH$_4$ variability in the troposphere and lower stratosphere, Atmos. Chem. Phys., 11, 12813–12837, https://doi.org/10.5194/acp-11-12813-2011, 2011.

Perrette, M.: ISI-MIP/isipedia-countries (v2.6), GitHub [data set], https://github.com/ISI-MIP/isipedia-countries/releases/tag/v2.6 (last access: 22 November 2024), 2023.

Prather, M.: Numerical advection by conservation of second-order moments, J. Geophys. Res., 91, 6671–6681, 1986.

Randel, W. J. and Park, M.: Deep convective influence on the Asian summer monsoon anticyclone and associated tracer variability observed with Atmospheric Infrared Sounder (AIRS), J. Geophys. Res., 111, D12314, https://doi.org/10.1029/2005JD006490, 2006.

Randel, W. J., Park, M., Emmons, L., Kinnison, D., Bernath, P., Walker, K. A., Boone, C., and Pumphrey, H.: Asian monsoon transport of pollution to the stratosphere, Science, 328, 611–613, https://doi.org/10.1126/science.1182274, 2010.

Roozitalab, B., Emmons, L. K., Hornbrook, R. S., Kinnison, D. E., Fernandez, R. P., Li, Q., Saiz-Lopez, A., Hossaini, R., Cuevas, C. A., Hills, A. J., Montzka, S. A., Blake, D. R., Brune, W. H., Veres, P. R., and Apel, E. C.: Measurements and modeling of the interhemispheric differences of atmospheric chlorinated very short-lived substances, J. Geophys. Res.-Atmos., 129, e2023JD039518, https://doi.org/10.1029/2023JD039518, 2024.

Saiz-Lopez, A., Baidar, S., Cuevas, C. A., Koenig, T., Fernandez, R. P., Dix, B., Kinnison, D. E., Lamarque, J.-F., Rodriguez-Lloveras, X., and Campos, T. L.: Injection of iodine to the stratosphere, Geophys. Res. Lett., 42, 6852–6859, https://doi.org/10.1002/2015GL064796, 2015.

Salawitch, R., Weisenstein, D., Kovalenko, L., Sioris, C., Wennberg, P., Chance, K., Ko, M., and McLinden, C.: Sensitivity of ozone to bromine in the lower stratosphere, Geophys. Res. Lett., 32, L05811, https://doi.org/10.1029/2004GL021504, 2005.

Sander, R.: Compilation of Henry's law constants (version 5.0.0) for water as solvent, Atmos. Chem. Phys., 23, 10901–12440, https://doi.org/10.5194/acp-23-10901-2023, 2023.

Say, D., Ganesan, A. L., Lunt, M. F., Rigby, M., O'Doherty, S., Harth, C., Manning, A. J., Krummel, P. B., and Bauguitte, S.: Emissions of halocarbons from India inferred through atmo-

spheric measurements, Atmos. Chem. Phys., 19, 9865–9885, https://doi.org/10.5194/acp-19-9865-2019, 2019.

Sherwood, J.: European restrictions on 1,2-dichloroethane: C-H activation research and development should be liberated and not limited, Angew. Chem. Int. Ed., 57, 14286–14290, https://doi.org/10.1002/anie.201800549, 2018.

Singh, H. B., Brune, W. H., Crawford, J. H., Flocke, F., and Jacob, D. J.: Chemistry and transport of pollution over the Gulf of Mexico and the Pacific: spring 2006 INTEX-B campaign overview and first results, Atmos. Chem. Phys., 9, 2301–2318, https://doi.org/10.5194/acp-9-2301-2009, 2009.

Simpson, I. J., Blake, D. R., Blake, N. J., Meinardi, S., Barletta, B., Hughes, S. C., Fleming, L. T., Crawford, J. H., Diskin, G. S., Emmons, L. K., Fried, A., Guo, H., Peterson, D. A., Wisthaler, A., Woo, J.-H., Barré, J., Gaubert, B., Kim, J., Kim, M. J., Kim, Y., Knote, C., Mikoviny, T., Pusede, S. E., Schroeder, J. R., Wang, Y., Wennberg, P. O., and Zeng, L.: Characterization, sources and reactivity of volatile organic compounds (VOCs) in Seoul and surrounding regions during KORUS-AQ, Elementa-Sci. Anthrop., 8, 37, https://doi.org/10.1525/elementa.434, 2020.

TEAP: UNEP 2022 Report Of The Medical And Chemical Technical Options Committee (MCTOC), Technology and Economic Assessment Panel, ISBN 978-9966-076-99-1, 2022.

Thompson, C. R., Wofsy, S. C., Prather, M. J., et al.: The NASA Atmospheric Tomography (ATom) Mission: Imaging the Chemistry of the Global Atmosphere, BAMS, 103, E761–E790, https://doi.org/10.1175/BAMS-D-20-0315.1, 2022.

UNEP: 1,2-Dichloroethane: SIDS Initial Assessment Report, United National Environment Programme, https://hpvchemicals.oecd.org/ui/handler.axd?id=95f8d194-732a-4cc9-b59b-839ed3b18732 (last access: 22 November 2024), 2002.

Villamayor, J., Iglesias-Suarez, F., Cuevas, C. A., Fernandez, R. P., Li, Q., Abalos, M., Hossaini, R., Chipperfield, M. P., Kinnison, D. E., Tilmes, S., Lamarque, J.-F., and Saiz-Lopez, A.: Very short-lived halogens amplify ozone depletion trends in the tropical lower stratosphere, Nat. Clim. Change, 13, 554–560, https://doi.org/10.1038/s41558-023-01671-y, 2023.

von Hobe, M., Grooß, J.-U., Günther, G., Konopka, P., Gensch, I., Krämer, M., Spelten, N., Afchine, A., Schiller, C., Ulanovsky, A., Sitnikov, N., Shur, G., Yushkov, V., Ravegnani, F., Cairo, F., Roiger, A., Voigt, C., Schlager, H., Weigel, R., Frey, W., Borrmann, S., Müller, R., and Stroh, F.: Evidence for heterogeneous chlorine activation in the tropical UTLS, Atmos. Chem. Phys., 11, 241–256, https://doi.org/10.5194/acp-11-241-2011, 2011.

Wang, C., Shao, M., Huang, D., Lu, S., Zeng, L., Hu, M., and Zhang, Q.: Estimating halocarbon emissions using measured ratio relative to tracers in China, Atmos. Environ., 89, 816–826, https://doi.org/10.1016/j.atmosenv.2014.03.025, 2014.

WMO: Scientific Assessment of Ozone Depletion: 2018, Global Ozone Research and Monitoring Project-Report No. 58, World Meteorological Organization, Geneva, Switzerland, ISBN 978-1-7329317-1-8, 2018.

WMO: Scientific Assessment of Ozone Depletion: 2022, Global Ozone Research and Monitoring Project, GAW Report No. 278, World Meteorological Organization, Geneva, Switzerland, ISBN 978-9914-733-97-6, 2022.

Wofsy, S. C., Team, H. S., Team, C. M., and Team, S.: HIAPER Pole-to-Pole Observations (HIPPO): fine-grained, globalscale measurements of climatically important atmospheric gases and aerosols, Philos. T. R. Soc., 369, 2073–2086, https://doi.org/10.1098/rsta.2010.0313, 2011.

Wofsy, S. C., Daube, B., Jimenez-Pizarro, R., Kort, E., Pittman, J. V., Park, S., Commane, R., Xiang, B., Santoni, G., Jacob, D. J., Fisher, J. A., Pickett-Heaps, C. A., Wang, H., Wecht, K. J., Wang, Q., Stephens, B. B., Shertz, S. R., Watt, A., Romashkin, P., Campos, T., Haggerty, J., Cooper, W. A., Rogers, D. C., Beaton, S., Hendershot, R., Elkins, J. W., Fahey, D. W., Gao, R.-S., Schwarz, J. P., Moore, F., Montzka, S. A., Perring, A. E., Hurst, D., Miller, B. R., Sweeney, C., Oltmans, S. J., Hintsa, E. J., Nance, D., Dutton, G. S., Watts, L. A., Spackman, J. R., Rosenlof, K. H., Ray, E., Hall, B., Zondlo, M., Diao, M., Keeling, R. K., Bent, J., Atlas, E., Lueb, R., and Mahoney, M. J.: HIPPO Combined Discrete Flask and GC Sample GHG, Halocarbon, and Hydrocarbon Data, Version 1.0, UCAR/NCAR – Earth Observing Laboratory [data set], https://doi.org/10.3334/CDIAC/HIPPO_012, 2017.

Wofsy, S. C., Afshar, S., Allen, H. M., Apel, E. C., Asher, E. C., Barletta, B., Bent, J., Bian, H., Biggs, B. C., Blake, D. R., Blake, N., Bourgeois, I., Brock, C. A., Brune, W. H., Budney, J. W., Bui, T. P., Butler, A., Campuzano-Jost, P., Chang, C. S., Chin, M., Commane, R., Correa, G., Crounse, J. D., Cullis, P. D., Daube, B. C., Day, D. A., Dean-Day, J. M., Dibb, J. E., DiGangi, J. P., Diskin, G. S., Dollner, M., Elkins, J. W., Erdesz, F., Fiore, A. M., Flynn, C. M., Froyd, K. D., Gesler, D. W., Hall, S. R., Hanisco, T. F., Hannun, R. A., Hills, A. J., Hintsa, E. J., Hoffman, A., Hornbrook, R. S., Huey, L. G., Hughes, S., Jimenez, J. L., Johnson, B. J., Katich, J. M., Keeling, R. F., Kim, M. J., Kupc, A., Lait, L. R., McKain, K., Mclaughlin, R. J., Meinardi, S., Miller, D. O., Montzka, S. A., Moore, F. L., Morgan, E. J., Murphy, D. M., Murray, L. T., Nault, B. A., Neuman, J. A., Newman, P. A., Nicely, J. M., Pan, X., Paplawsky, W., Peischl, J., Prather, M. J., Price, D. J., Ray, E. A., Reeves, J. M., Richardson, M., Rollins, A. W., Rosenlof, K. H., Ryerson, T. B., Scheuer, E., Schill, G. P., Schroder, J. C., Schwarz, J. P., St.Clair, J. M., Steenrod, S. D., Stephens, B. B., Strode, S. A., Sweeney, C., Tanner, D., Teng, A. P., Thames, A. B., Thompson, C. R., Ullmann, K., Veres, P. R., Wagner, N. L., Watt, A., Weber, R., Weinzierl, B. B., Wennberg, P. O., Williamson, C. J., Wilson, J. C., Wolfe, G. M., Woods, C. T., Zeng, L. H., and Vieznor, N.: ATom: Merged Atmospheric Chemistry, Trace Gases, and Aerosols, Version 2, ORNL DAAC [data set], Oak Ridge, Tennessee, USA, https://doi.org/10.3334/ORNLDAAC/1925, 2021.

Zou, H., Wang, T., Wang, Z. L, and Wang, Z.: Continuing large-scale global trade and illegal trade of highly hazardous chemicals, Nat Sustain., 6, 1394–1405, https://doi.org/10.1038/s41893-023-01158-w, 2023.